Stem Cell Reports
Article

OPEN ACCESS

A miRNA-Mediated Approach to Dissect the Complexity of Tumor-Initiating Cell Function and Identify miRNA-Targeting Drugs

Anil Belur Nagaraj,[1,11] Peronne Joseph,[1] Erin Ponting,[1] Yuriy Fedorov,[2] Salendra Singh,[1] Alex Cole,[3] Woncheol Lee,[3] Euisik Yoon,[3] Alessia Baccarini,[5] Peter Scacheri,[7] Ronald Buckanovich,[4] Drew J. Adams,[2,7] Ronny Drapkin,[6] Brian D. Brown,[5] and Analisa DiFeo[8,9,10,*]

[1]Case Comprehensive Cancer Center, Case Western Reserve University, Cleveland, OH 44106, USA
[2]Small Molecules Drug Development Core Facility, Office of Research Administration, Case Western Reserve University, Cleveland, OH 44106, USA
[3]Department of Electrical Engineering and Computer Science, Center for Wireless Integrated MicroSensing and Systems (WIMS2), The University of Michigan, Ann Arbor, MI, USA
[4]Department of Medicine, Magee Women's Cancer Research Center, UPMC Hillman Cancer Center, University of Pittsburgh, Pittsburgh, PA, USA
[5]Department of Genetics and Multiscale Biology, Icahn School of Medicine at Mount Sinai Hospital, New York, NY 10029, USA
[6]Penn Ovarian Cancer Research Center, Department of Obstetrics and Gynecology, Perelman School of Medicine, University of Pennsylvania, Pennsylvania, PA, USA
[7]Department of Genetics and Genomic Sciences, Case Western Reserve University, Cleveland, OH 44106, USA
[8]Rogel Cancer Center, The University of Michigan, Michigan Medicine, Ann Arbor, MI, USA
[9]Department of Obstetrics and Gynecology, The University of Michigan, Michigan Medicine, Ann Arbor, MI, USA
[10]Department of Pathology, The University of Michigan, Michigan Medicine, Ann Arbor, MI, USA
[11]Present address: Laboratory Medicine and Pathology, Mayo Clinic, Rochester, MN 55902, USA
*Correspondence: adifeo@med.umich.edu
https://doi.org/10.1016/j.stemcr.2018.12.002

SUMMARY

Tumor-initiating cells (TICs) contribute to drug resistance and tumor recurrence in cancers, thus experimental approaches to dissect the complexity of TICs are required to design successful TIC therapeutic strategies. Here, we show that miRNA-3′ UTR sensor vectors can be used as a pathway-based method to identify, enrich, and analyze TICs from primary solid tumor patient samples. We have found that an *miR-181a*^{high} subpopulation of cells sorted from primary ovarian tumor cells exhibited TIC properties *in vivo*, were enriched in response to continuous cisplatin treatment, and showed activation of numerous major stem cell regulatory pathways. This *miRNA*-sensor-based platform enabled high-throughput drug screening leading to identification of BET inhibitors as transcriptional inhibitors of *miR-181a*. Taken together, we provide a valuable miRNA-sensor-based approach to broaden the understanding of complex TIC regulatory mechanisms in cancers and to identify miRNA-targeting drugs.

INTRODUCTION

Tumor-initiating cells (TICs), or cancer stem cells, are subpopulations of cancer cells that are enriched in stem-like properties and drive tumor recurrence in various cancers (Bonnet and Dick, 1997; Al-Hajj et al., 2003; Kreso and Dick, 2014). Dissecting the complexities underlying TIC function is critical toward developing pharmacological strategies that can eradicate these cells. Several challenges in understanding TIC functions have emerged over the last few years as identified by various TIC studies across cancers, the most important of which in this context are TIC heterogeneity and TIC plasticity (Stewart et al., 2011; Meacham and Morrison, 2013). Enrichment of TICs based on pathway activity is an emerging approach in TIC research that offers a potential platform to study TICs in the context of heterogeneity and uncover therapies that selectively target this population of cells (Vermeulen et al., 2010; Tang et al., 2015). Existence of functional crosstalk between major stem cell regulatory pathways and the need for reliable indicators to determine the activity status of the pathway of interest in TIC clones as assessed in standard readout assays (e.g., flow cytometry/reporter assays) are main barriers in the pathway-based TIC study approach. Hence, identifying molecular entities that can regulate several pathways simultaneously coupled with reliable readout properties can greatly improve the understanding of TIC function in cancers. microRNAs (miRNAs) can be interesting candidates in this context and can offer study approaches that can potentially overcome the barriers in pathway-based TIC research.

miRNAs are small RNA molecules that mainly regulate post-transcriptional gene silencing by binding to the 3′ UTR of their potential targets, resulting in target mRNA degradation or translational repression (Ha and Kim, 2014). A single miRNA can thus affect multiple pathways and, not surprisingly, miRNAs are implicated in regulation of various aspects of tumorigenesis including regulation of TIC properties in many cancers (Yu et al., 2007; Shimono et al., 2009; Yin et al., 2010; Tung et al., 2017; Chen et al., 2017). Tumor subpopulations could be composed of cells with varying degrees of miRNA activity; hence, overexpression or knockdown of miRNAs to the same extent in all these populations may not reflect the true biology of miRNAs in these settings. Since 3′ UTR-driven activity is one of the defining traits of miRNA functions, isolation and characterization of TIC subpopulations in

cancers based on miRNA 3′ UTR activity can overcome the barriers associated with pathway-based approaches in TIC research. Isolating target cell populations based on miRNA activity using miRNA switches has been reported in physiological settings (Miki et al., 2015). Studying TICs in hematological malignancies utilizing a miRNA 3′ UTR activity-based approach has also been reported (Lechman et al., 2016). However, the application of miRNA activity-based tools to enrich for TICs in solid tumors or uncover miRNA-targeted drugs has not been explored to date.

Epithelial ovarian cancer (EOC) is the most lethal gynecological malignancy, in which TICs have been shown to be involved in the emergence of chemotherapy resistance and tumor recurrence, and to contribute to poor patient survival (Silva et al., 2011; Garson and Vanderhyden, 2015). One of the striking features of EOC is that even though the disease is heterogeneous in origin, the treatment approach has remained mostly homogeneous to date, i.e., platinum-based therapy has remained the mainstay of EOC treatment in the last few decades and resistance to platinum-based therapies continues to be the major barrier to eradication of this disease (Cunnea and Stronach, 2014). Thus, lack of TIC-targeted therapies may represent one of the main reasons for poor patient survival, and experimental approaches are required to dissect TIC function in order to develop drugs that could eradicate these cells. We have previously identified that high *miR-181a* expression correlates with poor survival in the high-grade serous ovarian cancer (HGSOC) subtype of EOC and that *miR-181a* is enriched in recurrent HGSOC tumors (Parikh et al., 2014). This correlation has also been shown in numerous other cancers (Pop-Bica et al., 2018). Most recently a comprehensive TCGA analysis of 12,000 tumor samples from 33 different cancers showed that a high level of *miR-181* family members correlated with an mRNA stemness signature (Malta et al., 2018), and *miR-181a* has been identified as a regulator of TICs in hepatic cancer (Ji et al., 2010), thus suggesting that this miRNA family could be involved in driving TIC properties. In the current study, we have developed a miRNA-sensor-based platform driven by *miR-181a* 3′ UTR activity to enrich TICs in primary EOC tumors and have identified *miR-181a* as a TIC therapeutic target. We further utilized the *miR-181a* sensor as a pharmacological screening platform to identify upstream regulators of *miR-181a* function, and uncovered that BET inhibitors transcriptionally regulate *miR-181a*.

RESULTS

miR-181a Induces Stem-like Properties in Non-transformed Fallopian Tube Secretory Epithelial Cells

Deregulation of adult stem cell drivers is one of the traits observed in TICs. Several regulators of TICs identified to date in cancers are in fact the ones that regulate stem-like properties under physiological conditions in their respective tissues (e.g., *LGR5*) (Barker et al., 2007; Shimokawa et al., 2017). Fallopian tube secretory epithelium (FTSE) has been identified as the origin of HGSOC, which is the most common subtype of EOC (Perets et al., 2013). Existence of a stem cell niche in the fallopian tube suggests a TIC-based origin of HGSOC (Flesken-Nikitin et al., 2013). Hence, identifying regulators of stem-like properties in FTSE cells can lead to characterization of TIC regulators in EOC. Thus, to investigate the potential role of *miR-181a* in driving TIC properties in EOC, we first looked at the effects of *miR-181a* upregulation in non-transformed FTSE cells (FTSE shp53-R24C) (Karst et al., 2011). We focused on *miR-181a*, given that this *miR-181* family member is the most highly expressed in HGSOC tumors (Figure S2A).

Upon stable *miR-181a* overexpression in FTSE cells we found increased expression of *ALDH1A1* and *CD133*, established as TIC markers in EOC (Figure 1A) (Choi et al., 2015). We next looked at sphere-initiating cell frequency in *miR-181a*-FTSE cells by utilizing *in vitro* limiting dilution tumor sphere-formation assay (Rota et al., 2012). Extreme limiting dilution analysis (ELDA) (Hu and Smyth, 2009) found that *miR-181a* increased sphere-initiating cell frequency by ~10-fold (Figures 1B and 1C). Conversely, stable downregulation of *miR-181a* decreased the expression of TIC markers *ALDH1A1*, *CD133*, and *LGR5* (Figure 1D), which was associated with an 18-fold decrease in sphere-initiating cell frequency in FTSE-*miR-181a* cells (Figure 1E), confirming specificity of *miR-181a* induced stem-like phenotype. Next, to assess whether *miR-181a* is a critical driver of TIC properties in EOC, we studied the effects of *miR-181a* overexpression on TIC properties in the OV81.2 primary HGSOC cell line model (Nagaraj et al., 2015a). OV81.2 cells exhibit high ALDH activity and form tumors at low cell numbers; however, tumor-initiation ability was significantly higher in OV81.2-*miR-181a* overexpressed cells as compared with OV81.2-control cells (~45-fold increase in tumor-initiating cell frequency, $p = 0.001$) (Figures 1F and 1G). These results support *miR-181a* as a regulator of stem-like properties in FTSE cells and primary HGSOC cells and suggest that *miR-181a* deregulation could underlie TIC function in EOC. Thus, we would predict that ovarian tumor cells with high *miR-181a* activity could potentially be enriched in TIC properties.

miR-181a Sensor Enriches for Tumor-Initiating Cells in Ovarian Cancer

We next set out to isolate *miR-181a*^{high} versus *miR-181a*^{low} subpopulation of tumor cells from ovarian tumors by using an miRNA sensor platform (Mullokandov et al., 2012). The

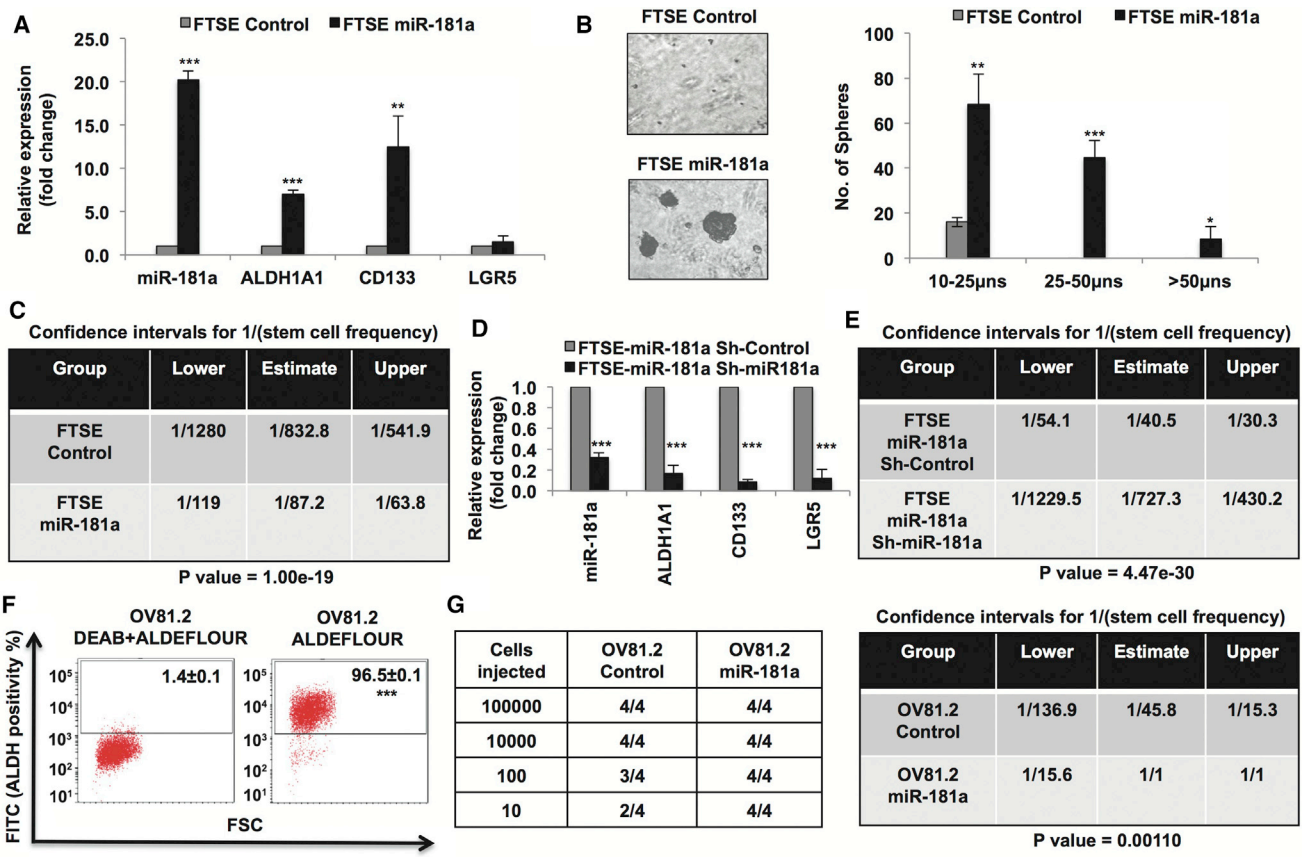

Figure 1. *miR-181a* Induces Stem-like Properties in Non-transformed Fallopian Tube Secretory Epithelial Cells

(A) Real-time PCR showing increased expression of stem cell markers in fallopian tube secretory epithelial (FTSE)-*miR-181a* cells.

(B) 3D-on-Top Matrigel sphere-formation assay. (Left) 5× light microscopy representative images showing increased sphere-formation by *miR-181a* overexpression (3 weeks) and (right) quantification of sphere size.

(C) *In vitro* limiting dilution sphere-formation assay (LDA) (3 weeks) showing ~10-fold increased sphere-initiating cell frequency upon *miR-181a* overexpression.

(D) Real-time PCR showing decreased stem cell markers upon *miR-181a* downregulation in FTSE-*miR-181a* cells.

(E) *In vitro* LDA assay (3 weeks) showing ~18-fold decreased sphere-initiating cell frequency upon *miR-181a* downregulation in FTSE-*miR-181a* cells.

(F) ALDEFLUOR flow-cytometry assay showing high ALDH activity in OV81.2 primary HGSOC PDX-derived cell line model (DEAB is an ALDH inhibitor).

(G) (Left) *In vivo* tumor-initiation assay showing *miR-181a* overexpression increases tumor-initiation ability in OV81.2 cells and (right) ELDA calculation of the tumor-initiating cell frequency showing ~45-fold increase in OV81.2-*miR-181a* cells as compared with OV81.2-control cells.

*p < 0.05, **p < 0.005, ***p < 0.005.

miR-181a sensor (Figure S1) enabled isolation of *miR-181a*^{high} and *miR-181a*^{low} cells from both OCI-P5X (primary HGSOC cells [Ince et al., 2015]) and HEYA8 (established TIC study model in ovarian cancer [Chau et al., 2013]) with ~4-fold increase in *miR-181a* expression (Figures 2A and 2B). Similar to what was observed in the TCGA dataset (Figure S2A), *miR-181a* was the predominant miRNA expressed in both *miR-181a*^{high} and *miR-181a*^{low} primary HGSOC OCI-P5X cells as compared with *miR-181b* and *miR-181c* (Figure S2B), whose expression levels were below reliable detectable levels. Hence, we focused on studying *miR-181a* in the current study. The ability to initiate tumors at low cell densities is a hallmark of TICs, thus we first looked at tumor-initiation capacity of *miR-181a* sensor-sorted OCI-P5X primary cells. OCI-P5X *miR-181a*^{high} cells were able to initiate tumors with as few as 1,000 cells whereas OCI-P5X *miR-181a*^{low} cells were unable to initiate tumors even at 100,000 cells (Figure 2C).

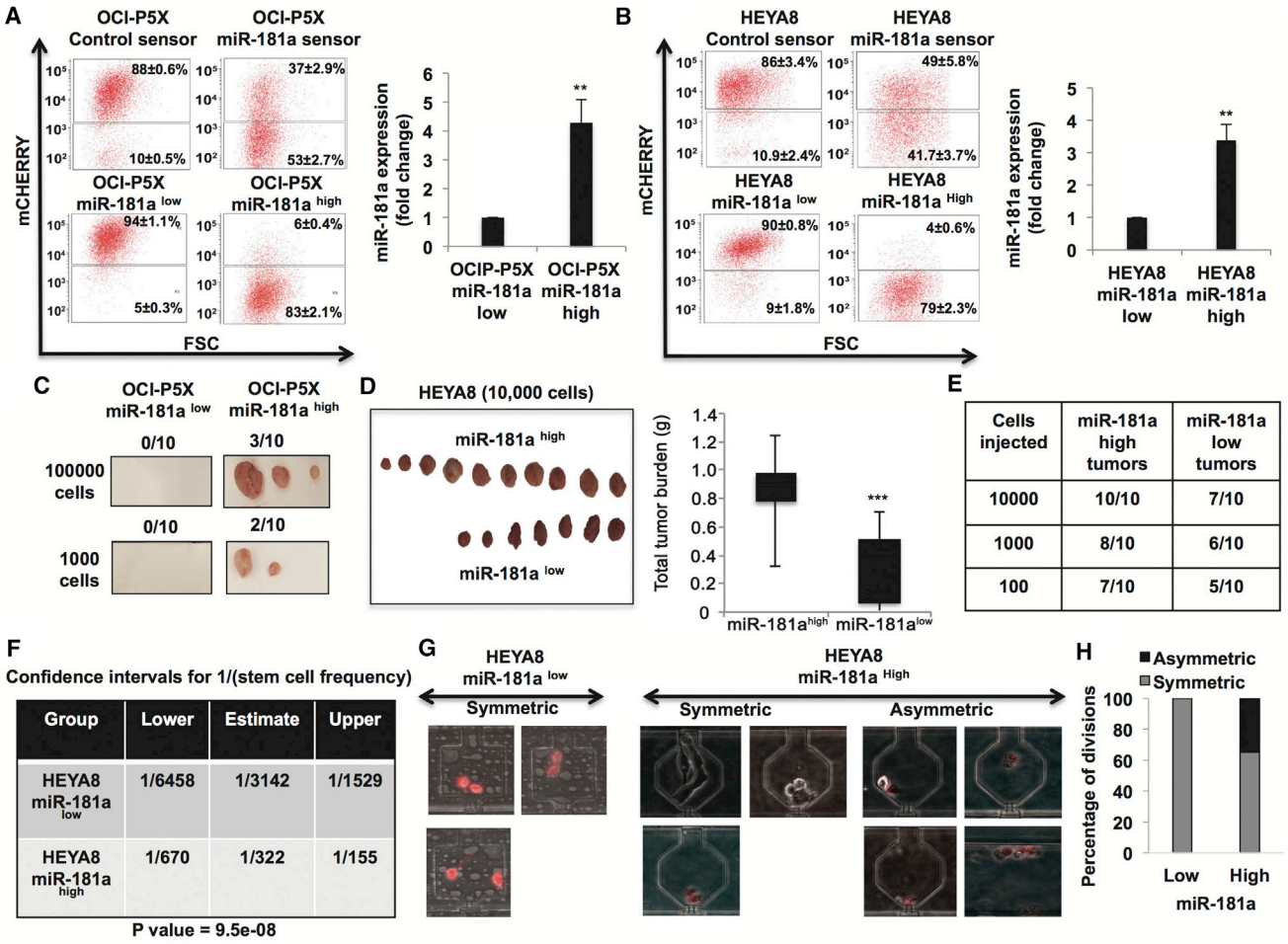

Cells injected	miR-181a high tumors	miR-181a low tumors
10000	10/10	7/10
1000	8/10	6/10
100	7/10	5/10

Group	Lower	Estimate	Upper
HEYA8 miR-181a low	1/6458	1/3142	1/1529
HEYA8 miR-181a high	1/670	1/322	1/155

P value = 9.5e-08

Figure 2. *miR-181a* Sensor Enriches for TICs in Ovarian Cancer

(A and B) *miR-181a* sensor-based sorting of mCherry^{high} and mCherry^{low} cells from OCI-P5X cells and HEYA8 cells (A, left and B, left) (sensor-sorted cells were analyzed three passages after sorting for reporter levels, and we did not observe changes in the reporter fluorescence activity even after 20 passages). Real-time PCR (A, right and B, right) showing ~4-fold difference in *miR-181a* expression in mCherry sorted cells.

(C) *In vivo* tumor initiation showing increased tumor formation by *miR-181a*^{high} primary HGSOC cells as compared with no tumors formed by *miR-181a*^{low} primary HGSOC cells at 100,000 cells (day 93) and 1,000 cells (day 121).

(D) *In vivo* tumor initiation showing increased tumor formation by *miR-181a*^{high} HEYA8 cells (10,000 cells) (day 35).

(E and F) *In vivo* LDA tumor-initiation assay (E) and ELDA analysis (F) showing increased tumor-initiating cell frequency (~10-fold) *in vivo* in *miR-181a*^{high} HEYA8 cells (day 28).

(G and H) Asymmetric and symmetric division of *miR-181a* sensor-sorted cells: top 10% *miR-181a*^{high} and *miR-181a*^{low} HEYA8 cells were sorted into single-cell-capture microfluidic devices and their growth was monitored daily for 15 days. Representative photomicrographs (G) of *miR-181a*^{low}/mCherry^{high} cell divisions showing these cells were only observed to divide to yield two *miR-181a*^{low}/mCherry^{high} cells. In contrast, miR-*181a*^{high}/mCherry^{low} cells divided both symmetrically to yield other mCherry-negative cells and asymmetrically to yield mCherry dim cells. (H) Summary of all divisions observed after 4 days of growth.

**p < 0.005, ***p < 0.005.

OCI-P5X *miR-181a*^{low} cells did not form tumors even after 121 days, suggesting it is unlikely that *181a*^{low} cells eventually produce tumors. HEYA8-*miR-181a*^{high} cells exhibited robust tumor formation (10/10) compared with HEYA8-*miR-181a*^{low} cells (7/10) (10,000 cells) (Figure 2D). Furthermore, *in vivo* limiting dilution tumor-initiation assays showed ~10-fold increase in tumor-initiating cell frequency in HEYA8 *miR-181a*^{high} cells (~1:322) compared with HEYA8 *miR-181a*^{low} cells (~1:3,142) (Figures 2E and 2F). *miR-181a* expression in *miR-181a*^{high} tumors was ~4-fold higher than that of *miR-181a*^{low} tumors (data not shown). This is similar to ~4-fold difference observed in

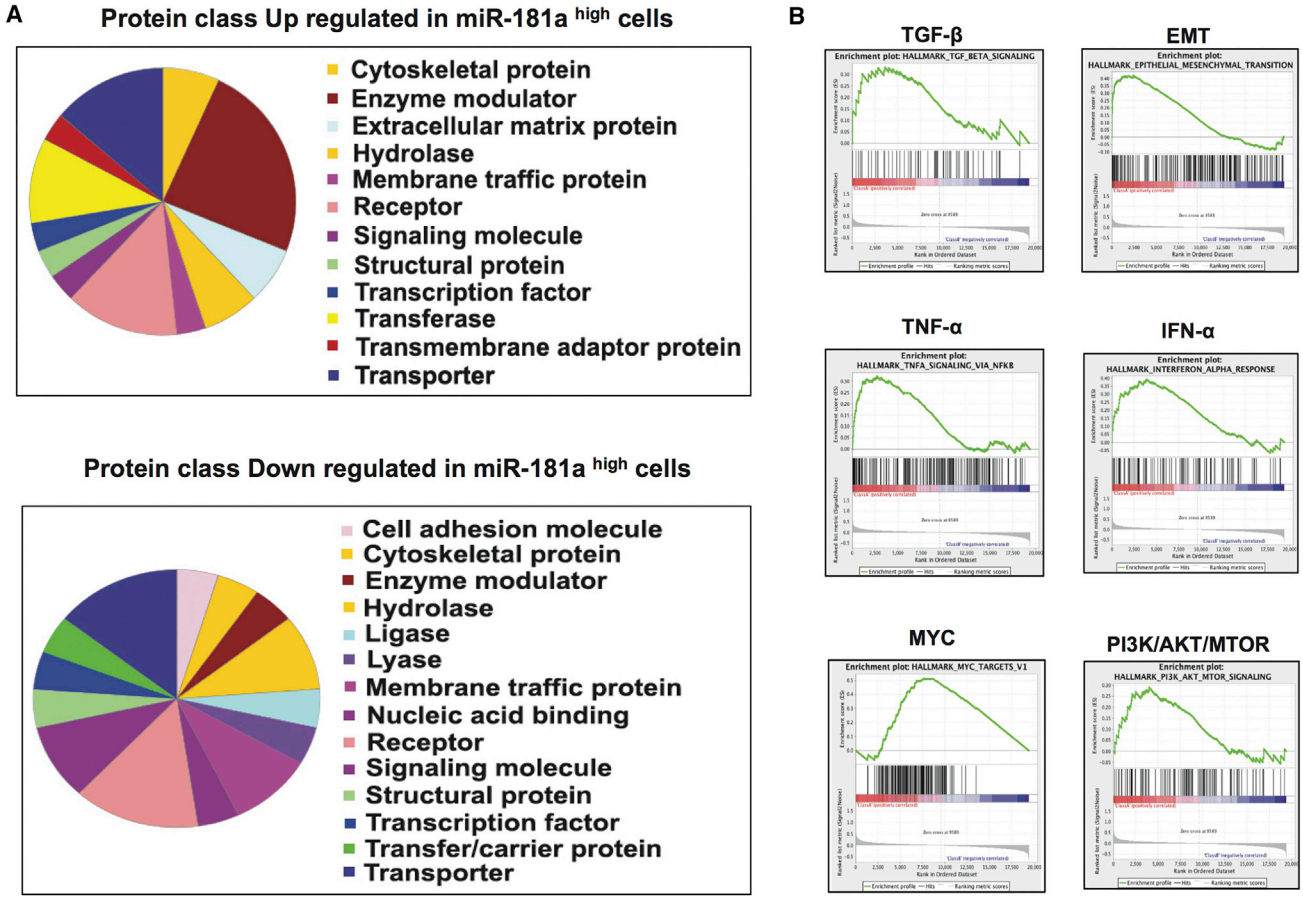

Figure 3. Pathways Enriched in *miR-181a*^{high} Primary HGSOC Cells

(A) PANTHER gene expression analysis of the top 50 genes upregulated or downregulated in *miR-181a*^{high} primary HGSOC (OCI-P5X) cells.
(B) GSEA analysis of the microarray data showing several TIC regulatory pathways enriched in *miR-181a*^{high} primary HGSOC (OCI-P5X) cells.

miR-181a expression between *miR-181a*^{high} and *miR-181a*^{low} cells *in vitro*. This suggests that *miR-181a*^{low} cells are unlikely to revert to *miR-181a*^{high} cells *in vivo*. We next assessed asymmetric cell division in these two populations, given that it is one of the defining traits of TICs and ovarian TICs are known to exhibit asymmetric cell division (Choi et al., 2015). We found that *miR-181a*^{low} ovarian tumor cells exhibited 100% symmetric cell division (relative to *miR-181a*) whereas *miR-181a*^{high} ovarian tumor cells exhibited both symmetric (~65%) and asymmetric (35%) divisions, further supporting that these cells are enriched in TIC properties (Figures 2G and 2H). *In vitro* proliferation rate did not differ between *miR-181a*^{low} and *miR-181a*^{high} ovarian tumor cells, confirming that the differences in TIC properties between these two populations are not due to differences in proliferation ability (Figure S3). Collectively, these results demonstrate the ability of miRNA 3′ UTR sensor to isolate TICs from primary tumors and also identify *miR-181a* as a regulator of TIC properties in EOC.

miR-181a Sensor Enriches for Multiple TIC Regulatory Signaling Pathways in Primary HGSOC Cells

Since the *miR-181a* sensor enabled isolation of ovarian TICs, we next looked at the pathways enriched in *miR-181a* sensor-sorted primary HGSOC cells by microarray analysis to determine the ability of miRNA sensor to potentially enrich for multiple TIC pathways. PANTHER gene expression analysis of the top 50 genes upregulated or downregulated in *miR-181a*^{high} primary HGOSC cells identified several classes of genes altered in these cells as compared with *miR-181a*^{low} primary HGSOC cells (Figure 3A). Furthermore, gene set enrichment analysis (GSEA) of the gene expression profile of *miR-181a*^{high} and *miR-181a*^{low} primary HGSOC cells revealed several known TIC regulatory pathways to be enriched in *miR-181a*^{high} cells, which correlated with the known fact that miRNAs regulate several pathways (Figure 3B). Epithelial mesenchymal transition (EMT) and transforming growth factor β (TGF-β) pathways were upregulated in *miR-181a*^{high} cells, which correlated with our previous results showing that

miR-181a induces EMT in ovarian cancer by activating TGF-β through the direct targeting of the inhibitory SMAD, SMAD7, thus confirming the functional reliability of the gene expression data (Parikh et al., 2014). In addition, several known stem cell regulatory pathways such as interferon-α (IFN-α), tumor necrosis factor α (TNF-α), PI3K/AKT/mTOR, and MYC were upregulated in *miR-181a*^{high} cells, showing that *miR-181a* sensor can enrich for multiple TIC regulatory pathways (Zhu et al., 2014; Lee et al., 2012; Xia and Xu, 2015; Dubrovska et al., 2009; Wang et al., 2008; Yang et al., 2017; Nair et al., 2014). The pathways enriched in *miR-181a*^{high} HGSOC cells could be due to combination of a direct effect of the miRNA and also an indirect effect due to potential crosstalks between the pathways. Therefore, we examined the top 100 downregulated genes in *miR-181a*^{high} HGSOC cells in comparison with *miR-181a* predicted targets (miRWalk database), which revealed that ∼30% of the downregulated genes in *miR-181a*^{high} HGSOC cells are predicted *miR-181a* targets (Table S1). Thus, enrichment of diverse TIC regulatory pathways directly or indirectly by *miR-181a* could contribute to increased TIC properties of *miR-181a*^{high} ovarian tumor cells.

miR-181a Sensor Enables Analysis of Ovarian Tumor Cell Response to Cisplatin in Real Time

The ability of TIC populations to survive standard cytotoxic chemotherapy leads to disease recurrence and poor outcomes. Thus, given that *miR-181a*^{high} ovarian tumor cells were enriched in TIC properties and *miR-181a* sensor provides a real-time platform to assess endogenous *miR-181a* activity, we utilized this platform to study the effects of long-term cisplatin treatment on *miR-181a* activity in ovarian tumor cells. Long-term culture of *miR-181a* sensor-transduced HEYA8 cells in the presence of cisplatin (HEYA8 *miR-181a*-sensor-CP10) increased the *miR-181a*^{high} subpopulation, which correlated with increased *miR-181a* expression (Figures 4A and 3B). Control sensor-transduced HEYA8 cells did not exhibit a decrease in the mCherry population upon long-term cisplatin treatment (HEYA8 control sensor-CP10) (Figure 4A). We next sorted mCherry^{high} and mCherry^{low} populations from HEYA8 *miR-181a*-sensor-CP10 cells (Figure 4C) and assessed their sphere-initiating cell frequency. HEYA8-*miR-181a*-sensor-CP10-mCherry^{low} (*miR-181a*^{high}) cells exhibited increased sphere-initiating cell frequency (∼12-fold) as compared with HEYA8-*miR-181a*-sensor-CP10-mCherry^{high} (*miR-181a*^{low}) cells, further confirming enrichment of *miR-181a*^{high} TICs in response to cisplatin treatment (Figure 4D). Long-term cisplatin treatment of *miR-181a*^{low} cells enriched the *miR-181a*^{high} subpopulation (HEYA8 *miR-181a*^{low} CP20) that correlated with increased *miR-181a* expression, suggesting enrichment of miR-*181a*^{high} cells in response to selection pressure induced by long-term treatment with cisplatin (Figures 4E and 4F). Next, we asked whether the miRNA 3′ UTR sensor platform would be able to isolate *miR-181a*^{high} ovarian tumor cells from primary recurrent HGSOC (OV236) tumor cells. We found that in this recurrent tumor the *miR-181a*^{high} subpopulation of cells exhibited the greatest difference in sphere-initiating cell frequency compared with all tumors tested. We observed a ∼20-fold increase in sphere-initiating cell frequency in the *miR-181a*^{high} compared with *miR-181a*^{low} cells (Figure 4G). These findings raise the possibility that targeting *miR-181a* could overcome the barrier of tumor recurrence by inhibiting TICs in EOC.

miRNA-Sensor-Based High-Throughput Therapeutic Screen Identifies BET Inhibitors as Potential Inhibitors of *miR-181a*

Even though transcriptional regulation of miRNAs forms a critical step in the regulation of miRNA functions, this aspect is not very well understood. Identifying upstream regulatory elements of miRNAs can lead to identification of inhibitors of these regulatory elements, thus greatly enhancing the efficacy of miRNA-targeted therapeutics. Current methodologies to study upstream regulatory elements of miRNAs are mainly limited to a candidate gene approach whereby selected genes/pathways are studied as potential drivers of miRNA expression, thus limiting the identification of miRNA inhibitors (Niu et al., 2016). The lack of reliable platforms to identify global regulators of miRNA transcription is the main barrier toward deciphering upstream regulatory elements involved in miRNA transcription. This, in turn, translates into the lack of miRNA-targeting drugs in oncology. Since our results identified *miR-181a* as a TIC therapeutic target in EOC, we next set out to test the utility of the miRNA sensor model as a tool to identify inhibitors of *miR-181a* that can be potentially evaluated as TIC-targeting drugs. For this approach, we first established a 384-well functional platform in which *miR-181a* inhibition in *miR-181a*^{high} (mCherry^{low}) ovarian tumor cells could be monitored as an increase in mCherry fluorescence readout (Figure S4). Using this 384-well platform, we treated the *miR-181a*^{high} ovarian tumor cells with a chemical library consisting of 3,114 compounds and looked for candidate drugs that increased mCherry fluorescence, thus identifying them as potential inhibitors of *miR-181a* expression (Table S2). Preliminary screening revealed 32 hits (Figure S5). Further correction for false-positive hits due to potential autofluorescence properties of the drugs translated into eight final hits (Figure 5A and Table S2). Interestingly, all eight hits have been previously linked with targeting TICs (Naujokat and Steinhart, 2012; Yokoyama et al., 2016) and SC144, an inhibitor *STAT3* that regulates

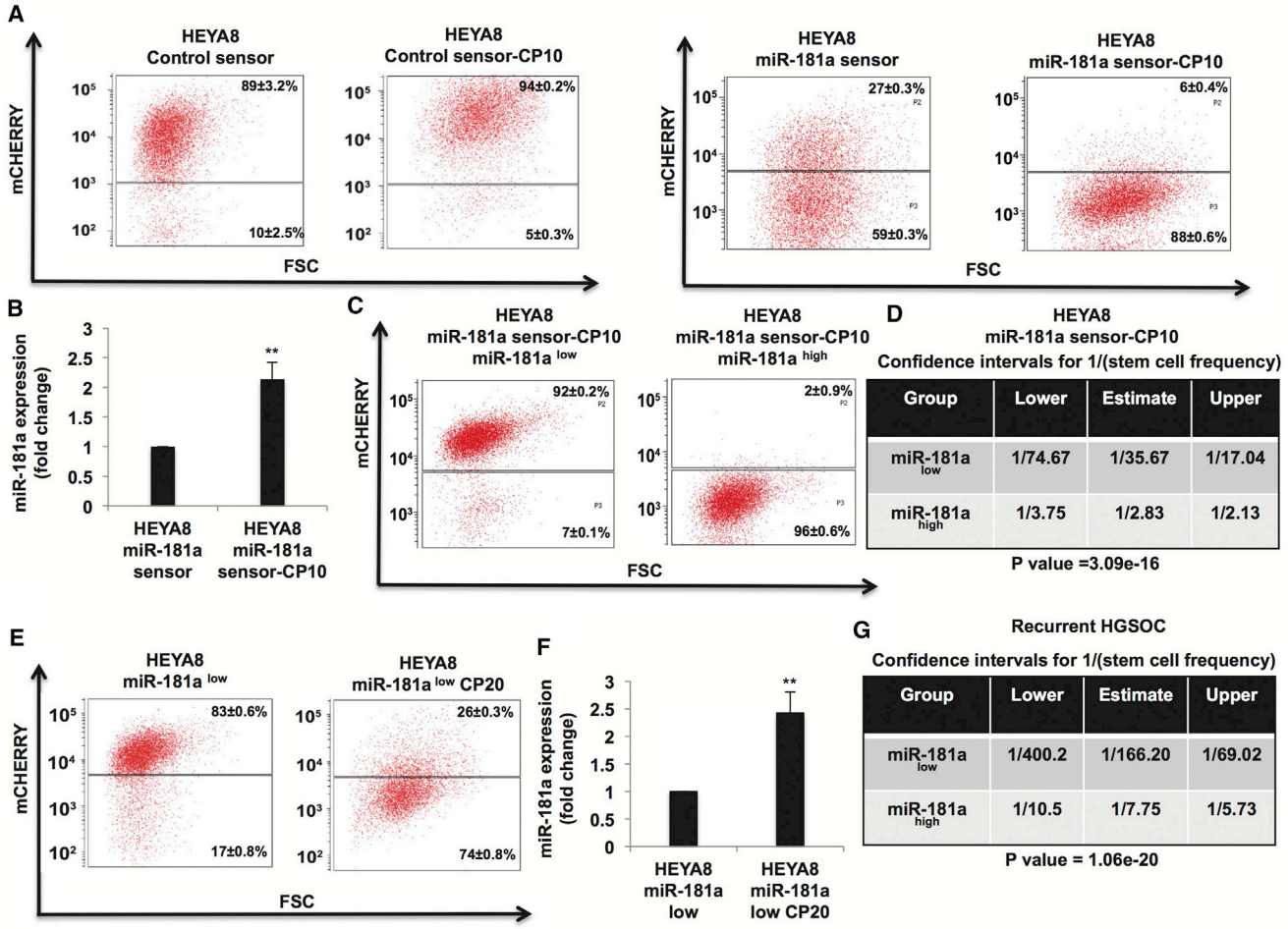

Figure 4. *miR-181a* Sensor Enables Analysis of Ovarian Tumor Cell Response to Cisplatin in Real Time

(A) Flow cytometry showing increase in *miR-181a*^{high} (mCherry^{low}) population in response to long-term cisplatin treatment (10 passages) in HEYA8 cells transduced with *miR-181a* sensor (right) compared with no decrease in mCherry fluorescence in control sensor-transduced HEY8 cells in response to long-term cisplatin treatment (2.5 μM) (left).

(B) Real-time PCR showing increased *miR-181a* expression in HEYA8-*miR-181a* sensor-CP10 cells.

(C and D) Flow cytometry (C) showing sorting of *miR-181a*^{high} (mCherry^{low}) and *miR-181a*^{low} (mCherry^{high}) subpopulations from HEYA8-*miR-181a* sensor-CP10 cells, and (D) *in vitro* LDA assay (3 weeks) showing increased sphere-initiating cell frequency (~12-fold) in *miR-181a*^{high} cells sorted from HEYA8-*miR-181a*-CP10 cells.

(E) Flow cytometry showing increased *miR-181a*^{high} subpopulation in response to long-term cisplatin treatment in HEYA8 *miR-181a*^{low} cells.

(F) Real-time PCR showing increased *miR-181a* expression in *miR-181a*^{low} cells upon long-term treatment with cisplatin.

(G) *In vitro* LDA assay (8 weeks) showing increased sphere-initiating cell frequency (~20-fold) in *miR-181a*^{high} cells sorted from primary recurrent HGSOC cells (OV236).

**p < 0.005.

miR-181a transcription (Niu et al., 2016), supports the functional reliability of the miRNA-sensor-screening platform. Furthermore, four of the eight hits were epigenetic regulators or bromodomain and extra-terminal motif (BET) inhibitors, suggesting an epigenetic regulation of *miR-181a* by the BET protein family that has not been reported to date in either cancer or normal physiological context.

We next assessed the correlation of cell counts versus mCherry fluorescence upon treatment with increasing doses of the identified eight hits. Six hits including the three BET inhibitors exhibited R^2 value of >0.7 in the correlation analysis, further suggesting that BET proteins could be regulators of *miR-181a* transcription (Figure 5B and Table S2). Sarcatinib and NSC319726 exhibited weak correlation and hence were excluded from further analysis. We

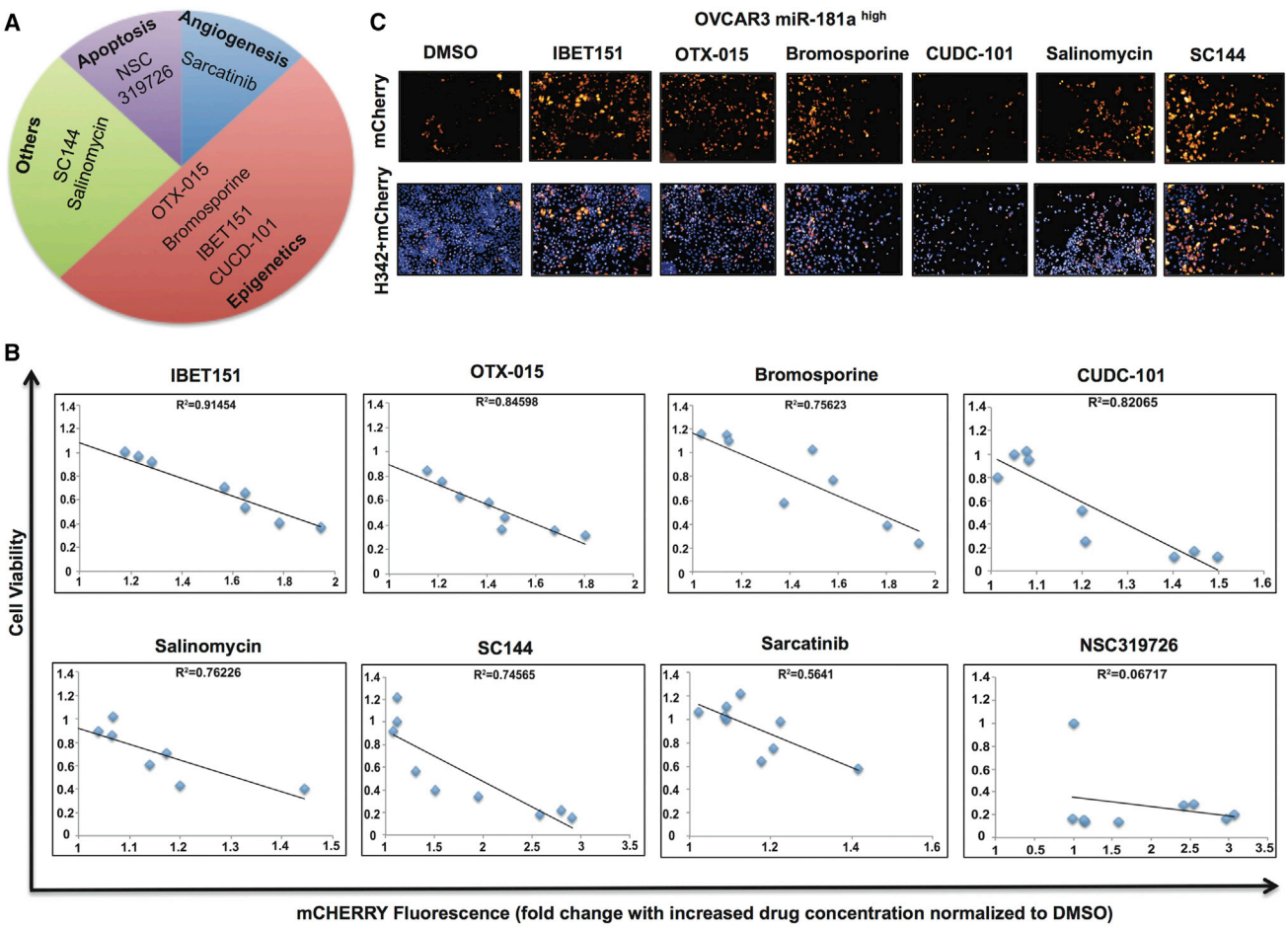

Figure 5. *miR-181a* Sensor Screen Identifies BET Inhibitors as Potential Inhibitors of *miR-181a*

(A) Final eight hits obtained from *miR-181a* sensor screen in OVCAR3 *miR-181a*^{high} cells showing epigenetic regulators as the main hits.

(B) Correlation analysis of mCherry fluorescence with cell counts upon treatment with all eight hits obtained from *miR-181a* sensor screen showing R^2 values >0.7 in 6 of the 8 hits.

(C) Fluorescence imaging of OVCAR3 *miR-181a*^{high} cells showing increased mCherry expression upon treatment with 6 of the 8 hits (10 μM 48 hr) with H342 dye used to detect viable cells.

further confirmed that these six hits increased mCherry expression in *miR-181a*^{high} cells (Figure 5C and Table S2).

miR-181a Is a Target of BET Inhibitors Across Cancers

We next set out to validate whether *miR-181a* is a target of BET inhibitors. BET inhibitors increased mCherry fluorescence in the *miR-181a*^{high} subpopulation sorted from OVCAR3, HEYA8, and primary HGSOC OCI-P5X cells, further validating the miRNA-sensor-screening results identifying BET inhibitors as inhibitors of *miR-181a* in EOC (Figure 6A). We subsequently confirmed that BET inhibitors decreased the expression of *miR-181a* by Taqman miRNA assays (Figure 6B). In addition, we looked at the effect of BET inhibition on *miR-181a* promoter activity (Presnell et al., 2015; Bert et al., 2000) to assess whether *miR-181a* is a transcriptional target of BET inhibitors. BET inhibitors decreased *miR-181a* promoter activity by ~70% in the *miR-181a*^{high} subpopulation sorted from OVCAR3, showing that *miR-181a* is a transcriptional target of BET inhibitors in EOC. Contrastingly, cisplatin increased *miR-181a* promoter activity in these cells by more than 1.5-fold, in accordance with the increased *miR-181a* expression seen in cisplatin-resistant EOC tumor cells (Figure 6C). Furthermore, BET inhibition decreased *miR-181a* promoter activity in the *miR-181a*^{high} subpopulation sorted from OCI-P5X (~90%) and HEYA8 cells (~80%), and also in FTSE cells (~90%) (Figure 6D). To assess whether *miR-181a* is a conserved target of BET proteins across cancers, we looked at the effect of BET inhibition on *miR-181a* promoter activity in breast cancer cells (MDA-MB-231) and lung cancer cells (H358). BET inhibition decreased *miR-181a* promoter activity in both breast cancer (~70%) and

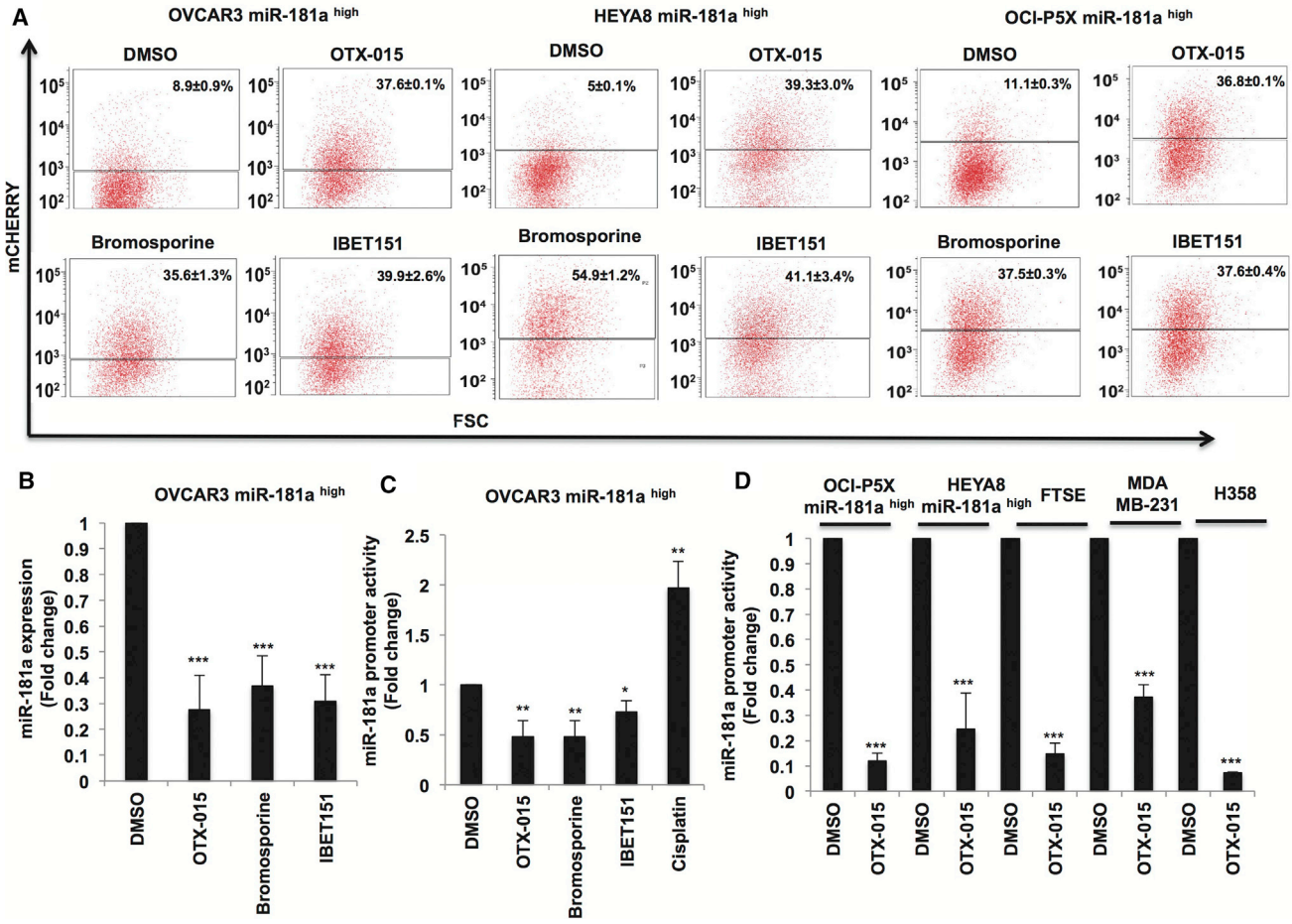

Figure 6. *miR-181a* Is a Target of BET Inhibitors

(A) Flow cytometry showing increased mCherry fluorescence upon treatment with BET inhibitors in *miR-181a*^{high} subpopulation sorted from OVCAR3-HEYA8 and OCI-P5X cells (10 μM, 48 hr).

(B) Real-time PCR showing decreased *miR-181a* expression upon treatment with BET inhibitors in OVCAR3-*miR-181a*^{high} cells (10 μM, 48 hr).

(C) *miR-181a* promoter reporter assay showing decreased promoter activity upon treatment with BET inhibitors (10 μM, 24 hr) and increased promoter activity by cisplatin (10 μM, 24 hr) in OVCAR3 *miR-181a*^{high} cells.

(D) *miR-181a* promoter reporter assay showing decreased promoter activity upon treatment with BET inhibitors (10 μM, 24 hr) in OCI-P5X *miR-181a*^{high} cells, HEYA8 *miR-181a*^{high} cells, FTSE cells, MDA-MB-231 cells, and H358 cells.

*p < 0.05, **p < 0.005, ***p < 0.005.

lung cancer cells (~90%), thus identifying a hitherto unknown function of BET protein family as regulators of *miR-181a* transcription across cancers (Figure 5D). Given that the mechanism of BET inhibitors is through the disruption of bromodomain proteins on to acetylated chromatin, we next examined whether the *miR-181a* promoter was acetylated. H3K27ac chromatin immunoprecipitation sequencing revealed that the *miR-181a* promoter was acetylated and, interestingly, this acetylation increased in cisplatin-resistant cells (Figure S6). Since *miR-181a* is implicated in regulation of various aspects of tumorigenesis across cancers, these results suggest that the BET-*miR-181a* axis could be a functionally conserved regulatory axis in cancers; hence, BET inhibitors could potentially be evaluated as small-molecule inhibitors of *miR-181a* function in cancers or *miR-181a* could be a potential biomarker for response.

DISCUSSION

Isolation, characterization, and targeting of TIC clones present in a tumor are a major barrier to complete eradication of all the cancer cells present in a patient. TIC regulators

can differ in patients due to intertumor and intratumor heterogeneity. An miRNA sensor approach can enhance the understanding of TIC functions in cancers because (1) miRNAs regulate multiple pathways, and thus miRNA activity can potentially enrich for multiple TIC clones in primary tumors, and (2) miRNA function can be assayed by 3′ UTR activity, and hence status of miRNA function can be reliably assayed in TIC clones in real time in response to genetic/pharmacological modulation.

Our results also demonstrate the importance of including non-transformed cell models to identify TIC regulators in cancers. Increased stem-like properties by *miR-181a* in non-transformed FTSE cells prompted us to investigate stem-like properties in *miR-181a*^{high} and *miR-181a*^{low} subpopulations in EOC tumors, thus identifying *miR-181a* as a regulator of TIC functions. Several predicted targets of *miR-181a* were enriched in *miR-181a*^{high} primary HGSOC cells. For example, PARK2 (Parkin), which was one of the predicted *miR-181a* targets that was downregulated in *miR-181a*^{high} HGSOC cells and has been characterized as a target of *miR-181a* in neuroblastoma cells (Cheng et al., 2016), is a negative regulator of PI3K/Akt pathways (Gupta et al., 2017). In addition, loss of PARK2 is reported to be associated with increased levels of cytokines such as TNF-α (Lee et al., 2016). Hence, downregulation of PARK2 in *miR-181a*^{high} HGSOC cells could be one of the mechanisms activating TNF-α and PI3K/Akt pathways in these cells. Furthermore, IRF8, which is a predicted *miR-181a* target downregulated in *miR-181a*^{high} cells, is a negative regulator of the IFN pathway and could contribute to the increased IFN-α pathway we observed in *miR-181a*^{high} HGSOC cells (White et al., 2016). Furthermore, ongoing studies in our laboratory have identified functional interaction of *miR-181a* with MYC in regulating HGSOC pathogenesis, which correlates with enrichment of the MYC pathway in *miR-181a*^{high} HGSOC cells (our unpublished data). In addition, it has been previously shown that *miR-181* is sharply induced in Myc-induced differentiated embryonic stem cells and tumor cells (Lin et al., 2009); thus, enrichment of the MYC pathway in the *miR-181a*^{high} HGSOC cells may be due to the upstream regulation of *miR-181a* by MYC. Activation of the Akt pathway by *miR-181a* has been reported, and hence this pathway could function downstream of *miR-181a* in HGSOC (Strotbek et al., 2017). Activation of PI3K/Akt pathway is known to induce MYC stabilization, and synergy between these two pathways is reported in cancers (Tsai et al., 2012; Sander et al., 2012), suggesting that crosstalk between enriched pathways could also be an important contributor to the increased TIC phenotype in *miR-181a*^{high} HGSOC cells.

In this study we have identified a hitherto unknown role of *miR-181a* in driving tumor recurrence in HGSOC, and show that (1) *miR-181a*^{high} ovarian tumor cells are enriched in TIC properties and (2) the *miR-181a*^{high} subpopulation of ovarian tumor cells is enriched in response to cisplatin treatment. *miR-181a* is reported to be induced by cisplatin treatment in lung cancer (Galluzzi et al., 2010), and our results show that cisplatin induces *miR-181a* promoter activity. Thus, both selection of *miR-181a*^{high} cells and induction of *miR-181a* in response to cisplatin treatment can contribute to enrichment of *miR-181a*^{high} cells upon cisplatin treatment. Moreover, *miR-181a* could be a common driver of both intrinsic stem-like properties in ovarian tumor cells, and also acquired stem-like properties in response to selection pressure induced upon cisplatin treatment. These data have been recently supported and expanded to other cancers through the comprehensive TCGA analysis of 12,000 tumor samples from 33 different cancers, which revealed that *miR-181* expression in several different cancers correlated with a high mRNA stemness index (Malta et al., 2018). Hence, *miR-181a* inhibition could be evaluated as an miRNA therapeutic approach targeting TICs to overcome the barrier of tumor recurrence in EOC as well as several other cancers.

One of the main barriers for advancements in miRNA therapeutics is the lack of in-depth understanding of transcriptional regulation of miRNAs in both physiological and cancer settings. Here, we have identified a role for BET inhibitors as miRNA modulators in EOC, in particular as *miR-181a* inhibitors. BET inhibitors are being explored as potential anti-cancer drugs in clinical trials across multiple cancers (Fujisawa and Filippakopoulos, 2017). BET inhibition is being evaluated as a potential therapeutic strategy in EOC, and BET inhibition is reported to decrease the expression of stemness-regulating genes and to overcome cisplatin resistance in EOC (Yokoyama et al., 2016). The *miR-181a*^{high} subpopulation in EOC could represent a potential TIC clone that could be targeted by BET inhibitors. However, since BET proteins regulate a multitude of cellular processes in cancers (Fujisawa and Filippakopoulos, 2017), several miRNAs could be targeted by BET inhibition in EOC. Changes in miRNAome induced by BET inhibition are not understood in EOC and, hence, functional characterization of miRNAome targeted by BET inhibitors in EOC is important to establish these drugs as miRNA-targeting drugs in EOC. Since miRNAs are established as reliable biomarkers in various cancers including EOC (Nagaraj et al., 2015b), miRNAs can be employed as biomarkers for both patient stratification and monitoring therapeutic efficacy of BET inhibition in EOC, thus enhancing the translational potential of BET inhibition in EOC with potential extension to other cancers.

By developing an miRNA-3′ UTR sensor platform and using it to explore the role of *miR-181a* in EOC, we have (1) simplified the understanding of functional complexity in TICs and expedited the journey toward near complete

isolation of multiple TIC clones in tumors, (2) identified a reliable approach to find small-molecule inhibitors of miRNA function that can greatly enhance the translational potential of miRNA therapeutics in both cancer and physiological contexts, and (3) uncovered a potential clinical biomarker for response to BET inhibitors.

EXPERIMENTAL PROCEDURES

Cell Culture and Reagents

Cells were cultured in 10-mm plates in a humidified atmosphere (5% CO_2) at 37°C. At 70%–90% confluence, trypsin (0.25%)/EDTA solution was used to detach the cells from the culture plate for passaging and used for further experiments until passage 20. FTSE cells (DMEM-F12 medium), OVCAR3, HEYA8, and H358 cells (RPMI medium), and MDA-MB-231 cells (DMEM medium) were cultured in their respective media supplemented with 10% fetal bovine serum (FBS) (Gibco) and 1% PenStrep (PS) (Gibco). Primary HGSOC cells (OCI-P5X, OV236) were cultured in OCMI-L medium (Liver Tumor Culture Core, University of Miami) supplemented with 2.5% heat-inactivated FBS (Gibco) and 1% PS. OCI-P5X cells were purchased from Liver Tumor Culture Core, University of Miami. Matrigel was purchased from Corning (NY). Cisplatin was purchased from Mount Sinai Hospital Pharmacy. *miR-181a* lentiviral overexpression and the control vector were purchased from Biosettia (San Diego, CA). *miR-181a* antagomiR lentiviral vector and the control vector were purchased from Genecopoeia (Rockville, MD). *miR-181a* antagomir and the corresponding negative control for transient transfections were purchased from Dharmacon. BET inhibitors were purchased from Selleckchem (Houston, TX).

Tumor-Initiating Cell Assays

For limiting dilution sphere assays, a BD FACSAria II sorter was used to sort cells directly into 96-well ultra-low attachment (ULA) plates (Corning, NY) in 200 μL of mammocult medium (STEMCELL Technologies, Vancouver, Canada) per well. After indicated time points, the number of wells with tumor spheres was counted and the data were analyzed by the ELDA platform to determine the sphere-initiating cell frequency. At each cell dosage three biological replicates were used for *in vitro* LDA assays. Each replicate was sorted in eight wells in ULA plates per cell dosage. For *in vivo* tumor-initiation assays, *miR-181a*^{high} and *miR-181a*^{low} cells were resuspended in cell culture medium with Matrigel in 50:50 ratios and injected subcutaneously in NU/NU mice, and tumor formation was assessed. For *in vivo* LDA assays, ten mice were studied in each group with OCI-P5X and HEYA8 cells, and four mice were studied in each group with OV81.2 cells. Tumor volume was estimated by standard caliper measurement ($V = L \times W^2/2$). The ELDA platform was employed to determine the tumor-initiating cell frequency. Symmetric and asymmetric cell division experiments were performed as described previously (Choi et al., 2015).

Statistical Analysis

Unless otherwise noted, data are presented as mean ± SD from three independent experiments, and Student's t test (two-tailed) was used to compare two groups ($p < 0.05$ was considered significant) for independent samples.

SUPPLEMENTAL INFORMATION

Supplemental Information includes Supplemental Experimental Procedures, six figures, and two tables and can be found with this article online at https://doi.org/10.1016/j.stemcr.2018.12.002.

AUTHOR CONTRIBUTIONS

A.D. and A.B.N. designed the study. A.B.N., P.J., and E.P. performed the experiments. Y.F. and D.J.A. performed the small-molecule screening. A.C., E.Y., and R.B. helped in performing the asymmetric cell division experiments. A.B. and B.D.B. designed, generated, and provided the *miR-181* 3′ UTR sensor vector. S.S. performed the GSEA analysis. R.D. provided the FTSE cell lines. A.D. and A.B.N. analyzed the results and wrote the manuscript. All authors reviewed the manuscript. A.D. supervised the overall study and finalized the manuscript.

ACKNOWLEDGMENTS

We thank Norma C. and Albert I. Geller for their constant support of the Gynecological Cancer Translational Research Program at Case Western Reserve University (A.D.). In addition, we thank Dr. Anirban Mitra for the HEYA8 cells, Dr. Goutham Narla for the MDA-MB-231 and H358 cells, and Dr. Steven Presnell for the *miR-181a* luciferase promoter. We acknowledge the help from Cytometry & Imaging Microscopy Core Facility and the Athymic Animal and Preclinical Therapeutics Core of the Case Comprehensive Cancer Center (P30CA043703). This work was supported by grants from The National Cancer Institute, R01CA197780 (A.D.), Department of Defense, OC150553 (A.D.), and The Young Scientist Foundation (A.D.).

Received: June 8, 2018
Revised: December 6, 2018
Accepted: December 6, 2018
Published: January 8, 2019

REFERENCES

Al-Hajj, M., Wicha, M.S., Benito-Hernandez, A., Morrison, S.J., and Clarke, M.F. (2003). Prospective identification of tumorigenic breast cancer cells. Proc. Natl. Acad. Sci. U S A *100*, 3983–3988.

Barker, N., van Es, J.H., Kuipers, J., Kujala, P., van den Born, M., Cozijnsen, M., Haegebarth, A., Korving, J., Begthel, H., Peters, P.J., et al. (2007). Identification of stem cells in small intestine and colon by marker gene Lgr5. Nature *449*, 1003–1007.

Bert, a G., Burrows, J., Osborne, C.S., and Cockerill, P.N. (2000). Generation of an improved luciferase reporter gene plasmid that employs a novel mechanism for high-copy replication. Plasmid *44*, 173–182.

Bonnet, D., and Dick, J.E. (1997). Human acute myeloid leukemia is organized as a hierarchy that originates from a primitive hematopoietic cell. Nat. Med. *3*, 730–737.

Chau, W.K., Ip, C.K., Mak, A.S.C., Lai, H.-C., and Wong, A.S.T. (2013). c-Kit mediates chemoresistance and tumor-initiating capacity of ovarian cancer cells through activation of Wnt/β-catenin-ATP-binding cassette G2 signaling. Oncogene *32*, 2767–2781.

Chen, M.W., Yang, S.T., Chien, M.H., Hua, K.T., Wu, C.J., Hsiao, S.M., Lin, H., Hsiao, M., Su, J.L., and Wei, L.H. (2017). The STAT3-miRNA-92-Wnt signaling pathway regulates spheroid formation and malignant progression in ovarian cancer. Cancer Res. *77*, 1955–1967.

Cheng, M., Liu, L., Lao, Y., Liao, W., Liao, M., Luo, X., Wu, J., Xie, W., Zhang, Y., and Xu, N. (2016). MicroRNA-181a suppresses parkin-mediated mitophagy and sensitizes neuroblastoma cells to mitochondrial uncoupler-induced apoptosis. Oncotarget *7*, 42274–42287.

Choi, Y.-J., Ingram, P.N., Yang, K., Coffman, L., Iyengar, M., Bai, S., Thomas, D.G., Yoon, E., and Buckanovich, R.J. (2015). Identifying an ovarian cancer cell hierarchy regulated by bone morphogenetic protein 2. Proc. Natl. Acad. Sci. U S A *112*, E6882–E6888.

Cunnea, P., and Stronach, E.A. (2014). Modeling platinum sensitive and resistant high-grade serous ovarian cancer: development and applications of experimental systems. Front. Oncol. *4*, 1–8.

Dubrovska, A., Kim, S., Salamone, R.J., Walker, J.R., Maira, S.-M., Garcia-Echeverria, C., Schultz, P.G., and Reddy, V.A. (2009). The role of PTEN/Akt/PI3K signaling in the maintenance and viability of prostate cancer stem-like cell populations. Proc. Natl. Acad. Sci. U S A *106*, 268–273.

Flesken-Nikitin, A., Hwang, C.-I., Cheng, C.-Y., Michurina, T.V., Enikolopov, G., and Nikitin, A.Y. (2013). Ovarian surface epithelium at the junction area contains a cancer-prone stem cell niche. Nature *495*, 241–245.

Fujisawa, T., and Filippakopoulos, P. (2017). Functions of bromodomain-containing proteins and their roles in homeostasis and cancer. Nat. Rev. Mol. Cell Biol. *18*, 246–262.

Galluzzi, L., Morselli, E., Vitale, I., Kepp, O., Senovilla, L., Criollo, A., Servant, N., Paccard, C., Hupé, P., Robert, T., et al. (2010). miR-181a and miR-630 regulate cisplatin-induced cancer cell death. Cancer Res. *70*, 1793–1803.

Garson, K., and Vanderhyden, B.C. (2015). Epithelial ovarian cancer stem cells: underlying complexity of a simple paradigm. Reproduction *149*, R59–R70.

Gupta, A., Anjomani-Virmouni, S., Koundouros, N., Dimitriadi, M., Choo-Wing, R., Valle, A., Zheng, Y., Chiu, Y.H., Agnihotri, S., Zadeh, G., et al. (2017). PARK2 depletion connects energy and oxidative stress to PI3K/Akt activation via PTEN S-Nitrosylation. Mol. Cell *65*, 999–1013.e7.

Ha, M., and Kim, V.N. (2014). Regulation of microRNA biogenesis. Nat. Rev. Mol. Cell Biol. *15*, 509–524.

Hu, Y., and Smyth, G.K. (2009). ELDA: Extreme limiting dilution analysis for comparing depleted and enriched populations in stem cell and other assays. J. Immunol. Methods *347*, 70–78.

Ince, T.A., Sousa, A.D., Jones, M.A., Harrell, J.C., Agoston, E.S., Krohn, M., Selfors, L.M., Liu, W., Chen, K., Yong, M., et al. (2015). Characterization of twenty-five ovarian tumour cell lines that phenocopy primary tumours. Nat. Commun. *6*, 7419.

Ji, J., Yamashita, T., Budhu, A., Forgues, M., Jia, H., Li, C., Deng, C., Wauthier, E., Reid, L.M., Ye, Q., et al. (2010). Identification of microRNA-181 by genome-wide screening as a critical player in EpCAM-positive hepatic cancer stem cells. Hepatology *50*, 472–480.

Karst, A.M., Levanon, K., and Drapkin, R. (2011). Modeling high-grade serous ovarian carcinogenesis from the fallopian tube. Proc. Natl. Acad. Sci. U S A *108*, 7547–7552.

Kreso, A., and Dick, J.E. (2014). Evolution of the cancer stem cell model. Cell Stem Cell *14*, 275–291.

Lechman, E.R., Gentner, B., Ng, S.W.K., Schoof, E.M., van Galen, P., Kennedy, J.A., Nucera, S., Ciceri, F., Kaufmann, K.B., Takayama, N., et al. (2016). MiR-126 regulates distinct self-renewal outcomes in normal and malignant hematopoietic stem cells. Cancer Cell *29*, 214–228.

Lee, S., She, J., Deng, B., Kim, J., de Andrade, M., Na, J., Sun, Z., Wampfler, J.A., Cunningham, J.M., Wu, Y., et al. (2016). Multiple-level validation identifies PARK2 in the development of lung cancer and chronic obstructive pulmonary disease. Oncotarget *7*, 44211–44223.

Lee, S.H., Hong, H.S., Liu, Z.X., Kim, R.H., Kang, M.K., Park, N.H., and Shin, K.H. (2012). TNFα enhances cancer stem cell-like phenotype via Notch-Hes1 activation in oral squamous cell carcinoma cells. Biochem. Biophys. Res. Commun. *424*, 58–64.

Lin, C.-H., Jackson, A.L., Guo, J., Linsley, P.S., and Eisenman, R.N. (2009). Myc-regulated microRNAs attenuate embryonic stem cell differentiation. EMBO J. *28*, 3157–3170.

Malta, T.M., Sokolov, A., Gentles, A.J., Burzykowski, T., Poisson, L., Weinstein, J.N., Kamińska, B., Huelsken, J., Omberg, L., Gevaert, O., et al. (2018). Machine learning identifies stemness features associated with oncogenic dedifferentiation. Cell *173*, 338–354.e15.

Meacham, C.E., and Morrison, S.J. (2013). Tumour heterogeneity and cancer cell plasticity. Nature *501*, 328–337.

Miki, K., Endo, K., Takahashi, S., Funakoshi, S., Takei, I., Katayama, S., Toyoda, T., Kotaka, M., Takaki, T., Umeda, M., et al. (2015). Efficient detection and purification of cell populations using synthetic MicroRNA switches. Cell Stem Cell *16*, 699–711.

Mullokandov, G., Baccarini, A., Ruzo, A., Jayaprakash, A.D., Tung, N., Israelow, B., Evans, M.J., Sachidanandam, R., and Brown, B.D. (2012). High-throughput assessment of microRNA activity and function using microRNA sensor and decoy libraries. Nat. Methods *9*, 840–846.

Nagaraj, A.B., Joseph, P., Kovalenko, O., Singh, S., Armstrong, A., Redline, R., Resnick, K., Zanotti, K., Waggoner, S., and DiFeo, A. (2015a). Critical role of Wnt/β-catenin signaling in driving epithelial ovarian cancer platinum resistance. Oncotarget *6*, 23720–23734.

Nagaraj, A.B., Joseph, P., and DiFeo, A. (2015b). miRNAs as prognostic and therapeutic tools in epithelial ovarian cancer. Biomark. Med. *9*, 241–257.

Nair, R., Roden, D.L., Teo, W.S., McFarland, A., Junankar, S., Ye, S., Nguyen, A., Yang, J., Nikolic, I., Hui, M., et al. (2014). C-Myc and Her2 cooperate to drive a stem-like phenotype with poor prognosis in breast cancer. Oncogene *33*, 3992–4002.

Naujokat, C., and Steinhart, R. (2012). Salinomycin as a drug for targeting human cancer stem cells. J. Biomed. Biotechnol. *2012*, 950658.

Niu, J., Xue, A., Chi, Y., Xue, J., Wang, W., Zhao, Z., Fan, M., Yang, C.H., Shao, Z.-M., Pfeffer, L.M., et al. (2016). Induction of miRNA-181a by genotoxic treatments promotes chemotherapeutic resistance and metastasis in breast cancer. Oncogene *35*, 1302–1313.

Parikh, A., Lee, C., Joseph, P., Marchini, S., Baccarini, A., Kolev, V., Romualdi, C., Fruscio, R., Shah, H., Wang, F., et al. (2014). microRNA-181a has a critical role in ovarian cancer progression through the regulation of the epithelial–mesenchymal transition. Nat. Commun. *5*, 2977.

Perets, R., Wyant, G.A., Muto, K.W., Bijron, J.G., Poole, B.B., Chin, K.T., Chen, J.Y.H., Ohman, A.W., Stepule, C.D., Kwak, S., et al. (2013). Transformation of the fallopian tube secretory epithelium leads to high-grade serous ovarian cancer in Brca;Tp53;Pten models. Cancer Cell *24*, 751–765.

Pop-Bica, C., Pintea, S., Cojocneanu-Petric, R., Del Sal, G., Piazza, S., Wu, Z.H., Alencar, A.J., Lossos, I.S., Berindan-Neagoe, I., and Calin, G.A. (2018). MiR-181 family-specific behavior in different cancers: a meta-analysis view. Cancer Metastasis Rev. *37*, 17–32.

Presnell, S.R., Al-Attar, A., Cichocki, F., Miller, J.S., and Lutz, C.T. (2015). Human natural killer cell microRNA: differential expression of MIR181A1B1 and MIR181A2B2 genes encoding identical mature microRNAs. Genes Immun. *16*, 89–98.

Rota, L.M., Lazzarino, D.A., Ziegler, A.N., LeRoith, D., and Wood, T.L. (2012). Determining mammosphere-forming potential: application of the limiting dilution analysis. J. Mammary Gland Biol. Neoplasia *17*, 119–123.

Sander, S., Calado, D.P., Srinivasan, L., Köchert, K., Zhang, B., Rosolowski, M., Rodig, S.J., Holzmann, K., Stilgenbauer, S., Siebert, R., et al. (2012). Synergy between PI3K signaling and MYC in burkitt lymphomagenesis. Cancer Cell *22*, 167–179.

Shimokawa, M., Ohta, Y., Nishikori, S., Matano, M., Takano, A., Fujii, M., Date, S., Sugimoto, S., Kanai, T., and Sato, T. (2017). Visualization and targeting of LGR5^{+} human colon cancer stem cells. Nature *545*, 187–192.

Shimono, Y., Zabala, M., Cho, R.W., Lobo, N., Dalerba, P., Qian, D., Diehn, M., Liu, H., Panula, S.P., Chiao, E., et al. (2009). Downregulation of miRNA-200c links breast cancer stem cells with normal stem cells. Cell *138*, 592–603.

Silva, I.A., Bai, S., McLean, K., Yang, K., Griffith, K., Thomas, D., Ginestier, C., Johnston, C., Kueck, A., Reynolds, R.K., et al. (2011). Aldehyde dehydrogenase in combination with CD133 defines angiogenic ovarian cancer stem cells that portend poor patient survival. Cancer Res. *71*, 3991–4001.

Stewart, J.M., Shaw, P.A., Gedye, C., Bernardini, M.Q., Neel, B.G., and Ailles, L.E. (2011). Phenotypic heterogeneity and instability of human ovarian tumor-initiating cells. Proc. Natl. Acad. Sci. U S A *108*, 6468–6473.

Strotbek, M., Schmid, S., Sánchez-González, I., Boerries, M., Busch, H., and Olayioye, M.A. (2017). miR-181 elevates Akt signaling by co-targeting PHLPP2 and INPP4B phosphatases in luminal breast cancer. Int. J. Cancer *140*, 2310–2320.

Tang, B., Raviv, A., Esposito, D., Flanders, K.C., Daniel, C., Nghiem, B.T., Garfield, S., Lim, L., Mannan, P., Robles, A.I., et al. (2015). A flexible reporter system for direct observation and isolation of cancer stem cells. Stem Cell Reports *4*, 155–169.

Tsai, W.B., Aiba, I., Long, Y., Lin, H.K., Feun, L., Savaraj, N., and Kuo, M.T. (2012). Activation of Ras/PI3K/ERK pathway induces c-Myc stabilization to upregulate argininosuccinate synthetase, leading to arginine deiminase resistance in melanoma cells. Cancer Res. *72*, 2622–2633.

Tung, S.L., Huang, W.C., Hsu, F.C., Yang, Z.P., Jang, T.H., Chang, J.W., Chuang, C.M., Lai, C.R., and Wang, L.H. (2017). miRNA-34c-5p inhibits amphiregulin-induced ovarian cancer stemness and drug resistance via downregulation of the AREG-EGFR-ERK pathway. Oncogenesis *6*, e326.

Vermeulen, L., De Sousa e Melo, F., van der Heijden, M., Cameron, K., de Jong, J.H., Borovski, T., Tuynman, J.B., Todaro, M., Merz, C., Rodermond, H., et al. (2010). Wnt activity defines colon cancer stem cells and is regulated by the microenvironment. Nat. Cell Biol. *12*, 468–476.

Wang, J., Wang, H., Li, Z., Wu, Q., Lathia, J.D., McLendon, R.E., Hjelmeland, A.B., and Rich, J.N. (2008). c-Myc is required for maintenance of glioma cancer stem cells. PLoS One *3*, e3769.

White, C.L., Kessler, P.M., Dickerman, B.K., Ozato, K., and Sen, G.C. (2016). Interferon regulatory factor 8 (IRF8) impairs induction of interferon induced with tetratricopeptide repeat motif (IFIT) gene family members. J. Biol. Chem. *291*, 13535–13545.

Xia, P., and Xu, X.-Y. (2015). PI3K/Akt/mTOR signaling pathway in cancer stem cells: from basic research to clinical application. Am. J. Cancer Res. *5*, 1602–1609.

Yang, A., Qin, S., Schulte, B.A., Ethier, S.P., Tew, K.D., and Wang, G.Y. (2017). MYC inhibition depletes cancer stem-like cells in triple-negative breast cancer. Cancer Res. *77*, 6641–6650.

Yin, G., Chen, R., Alvero, A.B., Fu, H.H., Holmberg, J., Glackin, C., Rutherford, T., and Mor, G. (2010). TWISTing stemness, inflammation and proliferation of epithelial ovarian cancer cells through MIR199A2/214. Oncogene *29*, 3545–3553.

Yokoyama, Y., Zhu, H., Lee, J.H., Kossenkov, A.V., Wu, S.Y., Wickramasinghe, J.M., Yin, X., Palozola, K.C., Gardini, A., Showe, L.C., et al. (2016). BET inhibitors suppress ALDH activity by targeting ALDH1A1 super-enhancer in ovarian cancer. Cancer Res. *76*, 6320–6330.

Yu, F., Yao, H., Zhu, P., Zhang, X., Pan, Q., Gong, C., Huang, Y., Hu, X., Su, F., Lieberman, J., et al. (2007). let-7 regulates self renewal and tumorigenicity of breast cancer cells. Cell *131*, 1109–1123.

Zhu, Y., Karakhanova, S., Huang, X., Deng, S.P., Werner, J., and Bazhin, A.V. (2014). Influence of interferon-α on the expression of the cancer stem cell markers in pancreatic carcinoma cells. Exp. Cell Res. *324*, 146–156.

Stem Cell Reports, Volume *12*

Supplemental Information

A miRNA-Mediated Approach to Dissect the Complexity of Tumor-Initiating Cell Function and Identify miRNA-Targeting Drugs

Anil Belur Nagaraj, Peronne Joseph, Erin Ponting, Yuriy Fedorov, Salendra Singh, Alex Cole, Woncheol Lee, Euisik Yoon, Alessia Baccarini, Peter Scacheri, Ronald Buckanovich, Drew J. Adams, Ronny Drapkin, Brian D. Brown, and Analisa DiFeo

Supplementary Methods

Lentiviral transduction

For lentiviral transfection, Lenti Starter Kit (System Biosciences, CA) was used. Briefly, $3x10^6$ 293T cells were plated in 10cm plate with antibiotic free DMEM media supplemented with 10% FBS. At 50-70% confluence, 2μg of lentiviral plasmid and 10μg of pPACKH1-plasmid mix were co-transfected with Lipofectamine 2000 (Life Technologies, CA) following manufacturer's protocol. 48hr later, virus particles were harvested and precipitated. Target cells were transduced by plating 100,000 cells/well in a 6 well plate with virus particles and 4μg/mL polybrene (Santa Cruz Biotechnologies, CA) and were analyzed 72 hrs later.

RNA extraction and real-time PCR

Total RNA was extracted using the Total RNA Purification Plus Kit (Norgen Biotek, ON, Canada) according to manufacturer's instructions. For mRNA analysis, cDNA synthesis from 1μg of total RNA was done using the Transcriptor Universal cDNA Master kit (Roche, IN, USA). SYBR green-based Real-time PCR was subsequently performed in triplicate using SYBR green master mix (Roche) on the Light Cycler 480 II real time PCR machine (Roche). For miRNA expression assays, cDNA synthesis was done using Taqman gene expression assays (Life Technologies, Carlsbad, CA) and subsequent Real-time PCR was performed using Taqman universal PCR mastermix, no AmpErase UNG buffer (Life Technologies, Carlsbad, CA) with corresponding probes and primer mix (Taqman gene expression assays).

Transient transfection assays

For *miR-181a* promoter assays, *miR-181a* promoter (1µg) and renilla (150ng) were co-transfected using lipofectamine RNAiMAX (Life Technologies). Luciferase activities were analyzed using the Dual-Luciferase Reporter Assay System (Promega) with data normalization to the corresponding renilla values. For *miR-181a* antagomiR experiments, the control antagomiR and *miR-181a* antagomiRs were both purchased from Dharmacon. OVCAR3 cells were transfected with 50nM of the antagomiRs using lipofectamine RNAiMAX. 24hrs after transfection the cells were plated in 384 well imaging plates at different cell densities and mCherry fluorescence was determined 24hrs later.

3D on top matrigel sphere formation assay

250µl matrigel was plated in 24 well plates (Corning) and after 30 min incubation at 37^0C, 5000 cells were plated in 250µl mammocult on top of the first matrigel layer and incubated at 37^0C for 1hr after which 500µl of 10% matrigel in mammocult was added on top. After 3 weeks, 10x10 stitch imaging was done at 10x (100 random images acquired) using a Retiga Aqua Blue camera (Q Imaging, Vancouver, BC) connected to a Leica DMI6000 inverted microscope. Individual images were taken and then a composite image was generated using the scan slide function in Metamorph Imaging Software (Molecular Devices, Downington, PA). Subsequent integrated analysis also used Metamorph software.

ALDEFLOUR Assay

ALDH activity was determined by using ALDEFLOUR assay kit (Stem cell technologies). Briefly, $1x10^6$ OV81.2-Control and OV81.2-*miR181a* cells were resuspended in ALDEFLOUR reagent at 37^0c for 45 minutes (after trypsinization and

PBS wash) in the presence or absence of the ALDH inhibitor DEAB. Flow data was acquired using LSRII (BD Biosciences).

microarray and GSEA analysis

Total RNA was extracted from cell lysates of OCI-P5X *miR-181a* ^{high} and OCI-P5X *miR-181a* ^{low} cells in triplicate and submitted for Microarray using Affymetrix Human Clariom S array and the WT Plus chemistry. In brief, for the WT Plus assay, 150ng of total RNA was labeled using a reverse transcription priming method to prime the entire length of each RNA transcript, including both polyA and non-polyA mRNA to provide complete and unbiased transcriptome coverage. This protocol efficiently generated amplified and biotinylated sense-stranded DNA targets, avoiding loss of specificity due to antisense strand interference. Data was check for quality before being assessed on the Affymetrix Clariom S Human MicroArray. Changes in mRNA expression were then identified using the Clariom S Human MicroArray. On this array expression for each gene was assessed by approximately 11 probes, which were tiled throughout the transcript. The array provides basic gene level coverage of known genes. Labeled samples were hybridized to the arrays overnight in a rotating Hybridization Oven. Arrays were stained and washed in Affymetrix FS45U Fluidics Stations according to Affymetrix automated procedures. Data is collected using the GC3000 scanner with autoloader. The Clariom S Assays for the microarray data were downloaded and all data has been uploaded to GEO (Accession GSE52077). The data was pre-processed with RMA (Robust multichip average algorithm) using the R/Bioconductor package *Oligo* (42) where background subtraction, quantile normalization, and summarization (via median-polish) was accomplished. Gene set Enrichment Analysis was performed between the 3

mCherry High samples and 3 mCherry low Controls, using the *web application of GSEA at Broad website*(43) with the Hallmark Gene sets that represents established biological states and Processes and shows coherent expression(44).

miR-181a promoter acetylation analysis

H3K27ac ChIP with rabbit anti-H3K27ac (Abcam no. 4729) was performed using 10 million cross-linked cells and sequencing libraries were prepared as previously described (Schmidt et al, Methods, 2009). ChIP–seq libraries were sequenced on a HiSeq 2500 platform at the Case Western Reserve University Genomics Core Facility. Data analysis was performed as previously described (Morrow et al, Nature Medicine 2018).

Screening with chemical library

Chemical Compounds

The Collection of Biologically Active Molecules (Collection3114) was compiled from LOPAC library (Millipore Sigma, USA) and Bioactive Compound Library (Selleckchem). A total of 3114 mechanistically annotated partially redundant compounds were used for screening. All compounds were dissolved in DMSO at 10mM. A final DMSO concentration of 0.1% was not exceeded in the screening assay and in hit validation experiments. Upon hit identification, all compounds were retested as 10mM stock solutions purchased from original vendor.

Measurement of drug activity

Both mCherry^{low} and mCherry^{high} cells were seeded at 600 cells/well in Corning 3712 384-well plates using growth media. Cells were seeded in 50μL of media using

automated dispenser (MultiFlo FX, BioTek). During screening campaign, a single column (16 wells) on each plate were seeded with mCherry^{high} cells and served as positive control and another single column was seeded with Cherry^{low} cells to serve as a negative control. The negative and positive controls contained the same percentage of vehicle. During re-screening in each plate, two columns (32 wells) on each plate were seeded with mCherry^{high} cells and served as positive control and another two columns were seeded with Cherry^{low} cells to serve as a negative control. For the screening, 384-well assay plates were prepared with final test concentrations of 10μM using a Janus liquid handling platform (Perkin Elmer) equipped with 50nL pin transfer tool (V&P Scientific). For hit validation in dose–response studies at eight concentrations in two-fold dilutions, final test plates were prepared from stock solutions at 10 mM using Janus liquid handling platform (Perkin Elmer) equipped with a standard 96 tip head. In both screening and hit validation experiments cells were incubated with compounds for 48 hr. After incubation cells were fixed with 2% paraformaldehyde and stained with nucleic acid binding dye Hoechst 33342 (H342, Millipore Sigma, 5μg/mL). To test possible auto-fluorescence of hit candidate compounds dose–response studies were also performed in untransfected human osteosarcoma cells U2OS.

Cell imaging and image analysis

Fixed and stained cells were subjected to imaging and image analysis. The Operetta high-content imaging system with a 10x objective (PerkinElmer) was used for cell imaging. mCherry [Ex(560-580)/Em(590-640)] and Hoechst [Ex(360-400)/Em(410-480)] fluorescent images were obtained from a single field for each well. Image acquisition and storage were performed using Harmony 4.1 and Columbus software suites (PerkinElmer).

Image analysis and calculations were performed using Acapella software suite (PerkinElmer). Cells nuclei were identified based on fluorescence intensity (FI) of DNA-bound H342 as well as shape and area. Cell number was then determined for each well. Relative viability was calculated on per-plate basis as follows: Viability = $CN_{compound}/MEAN\_CN_{vehicle}$, where $CN_{compound}$ is a cell number for a given compound treated well and $MEAN\_CN_{vehicle}$ is an average (N=16) of DMSO-only treated wells on that particular plate. Cell cytoplasm was detected around each nucleus using low-intensity RNA-bound H342 stain. After that, for each cell mCherry fluorescence intensity was determined within cytoplasm mask. Relative mCherry FI was calculated for each well as follows: $mCherry\_FI_{compound}/MEAN\_mCherry\_FI_{vehicle}$, where $mCherry\_FI_{compound}$ is an average mCherry FI for a given compound treated well and $MEAN\_mCherry\_FI_{vehicle}$ is an average (N=16) of DMSO-only treated wells on that particular plate.

Figure S1 Illustration of miR-181a sensor platform

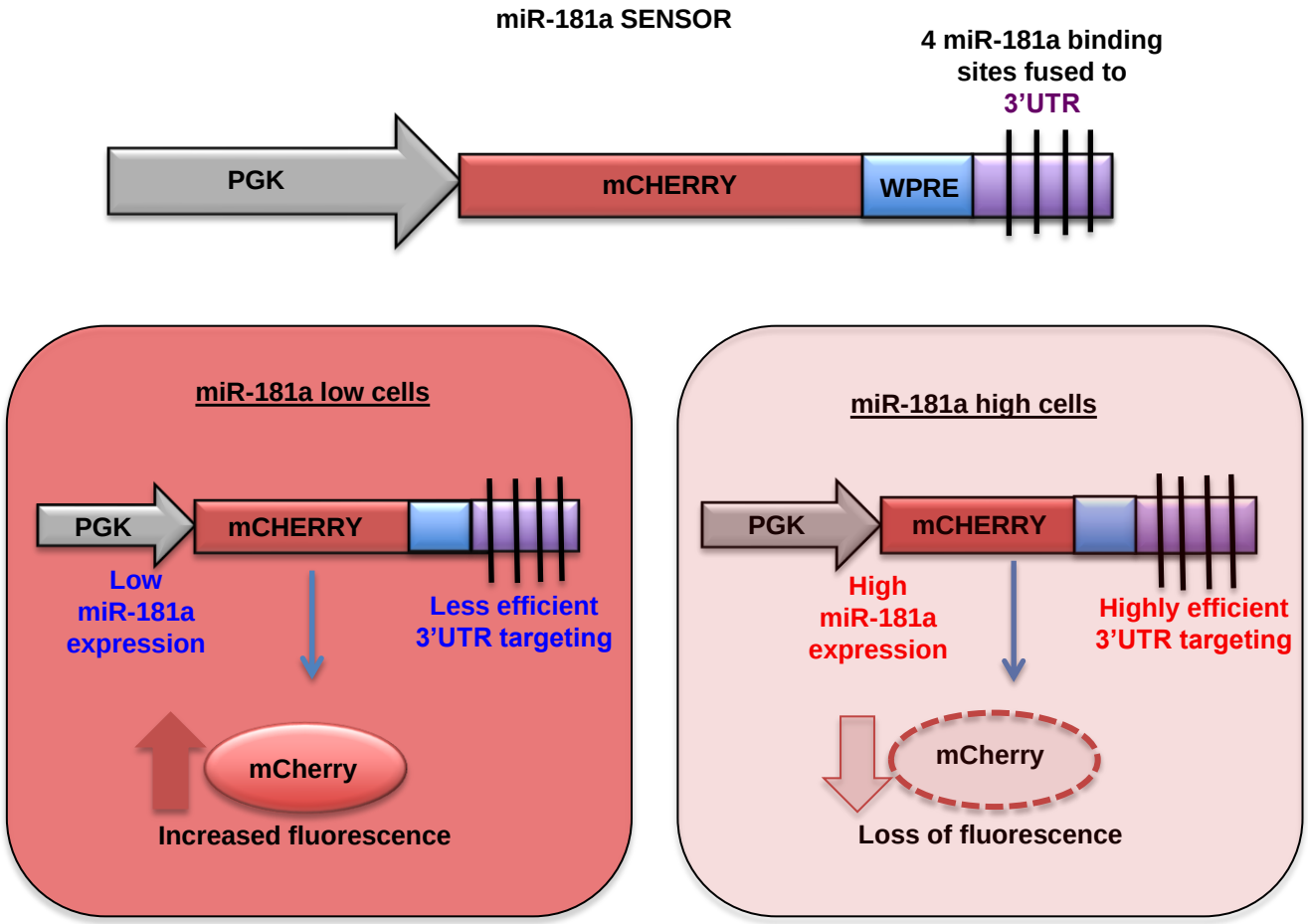

The *miR-181a* sensor contains 4 miR-181 recognition elements in the 3'UTR of mCherry. In this sensor the 3'UTR activity inversely correlates with mCherry fluorescence. Hence, low mCherry expression would represent the *miR-181a*^{high} population of cells. Conversely, high mCherry expression would represent the *miR-181a*^{low} population of cells that can be sorted out by transducing tumor cells with the *miR-181a* sensor.

Figure S2 Relative expression of miR-181 family members in TCGA cohort and OCI-P5X primary HGSOC cells

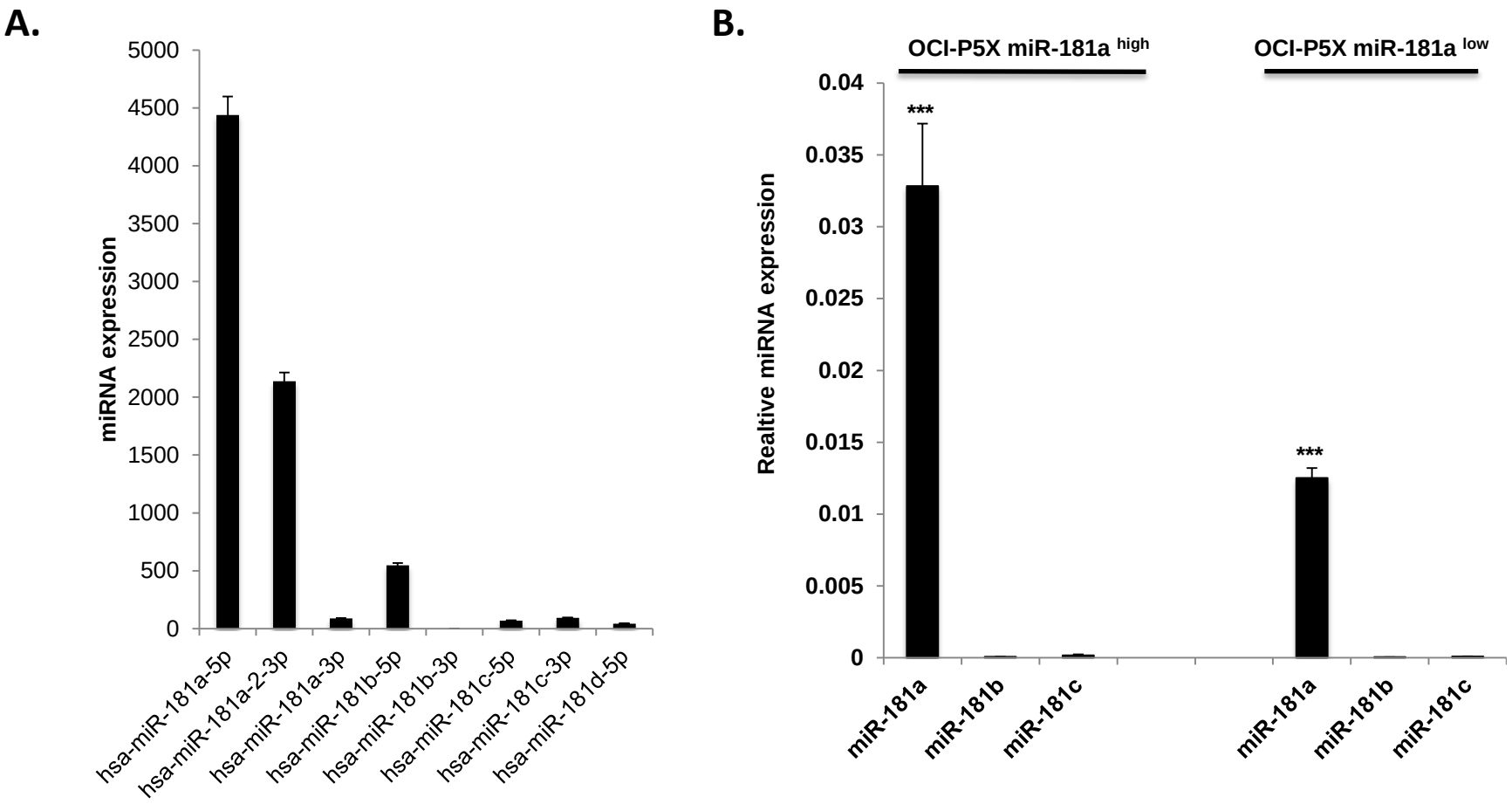

A. TCGA analysis of 476 HGSOC tumors revealed that miR-181a-5p and miR-181a-2-3p were the most highly expressed miR-181 family members. **B.** Taqman miRNA expression assay (three-independent experiments) showing significantly higher expression of *miR-181a* as compared to *miR-181b* and *miR-181c* in *miR-181a* sensor sorted primary HGSOC cells (*** $p<0.0005$) (Student's *t*-test two-tailed).

Figure S3 miR-181a ^{high} and miR-181a ^{low} cells do not differ in *in-vitro* proliferation rate

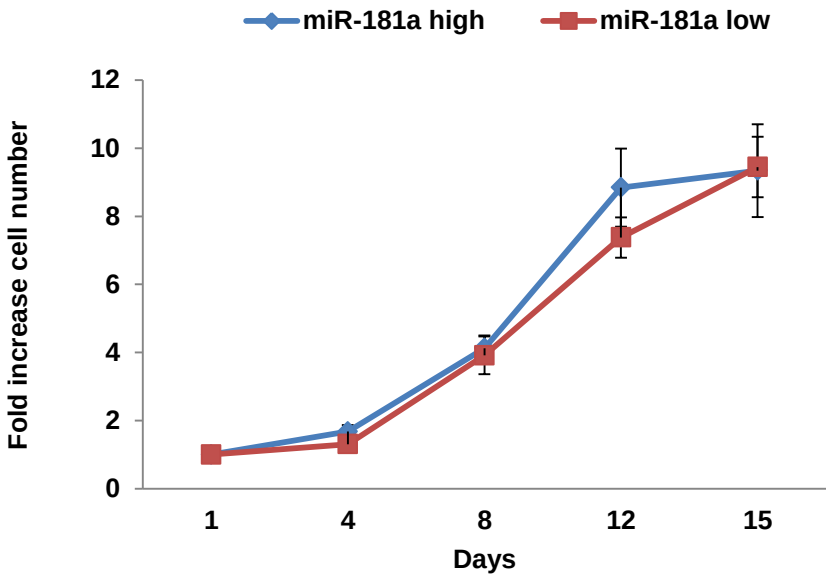

Growth curves for HEY miR-181a ^{low} and miR-181a ^{high} cells in microfluidic culture over 15 days. For these studies, a photograph was taken of each well of the plate on the indicated days. Total cell number is counted manually in the first 40 wells of each plate. Wells which had either no cell, 2 cells, or a contaminating cell (miR-181a low cell that contaminated the facs ~1% of cells) captured on the first day were excluded from analysis. Three independent isolates for each genotype were measured. The plots show mean ± SEM

Figure S4 Establishing *miR-181a* sensor based screening platform

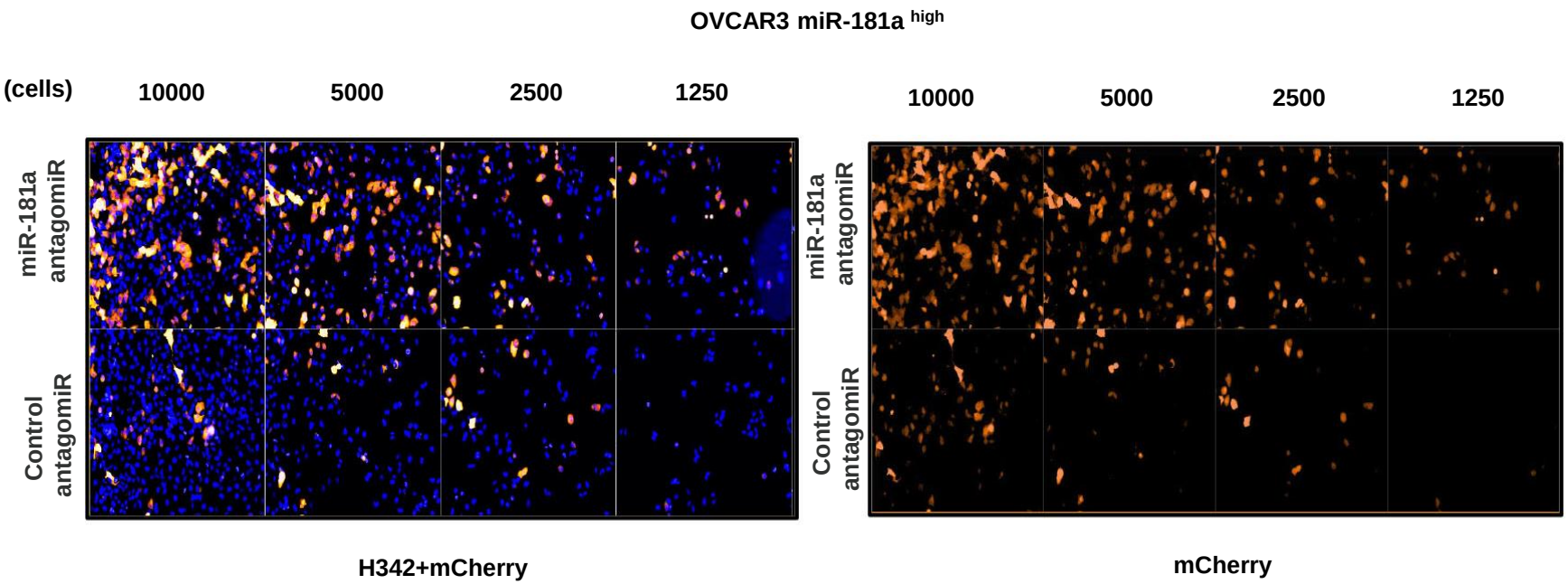

Fluorescence imaging showing increased mCherry fluorescence upon transfection with *miR-181a* antagomiR (50nM) (, *miR-181a* antagomiR was purchased from Dharmacon, Lipofectamine 2000 transfection protocol was used) as compared to control antagomiR in OVCAR3 cells. H342 dye was used to visualize cell nuclei.

Figure S5 32 Preliminary hits obtained from *miR-181a* screen

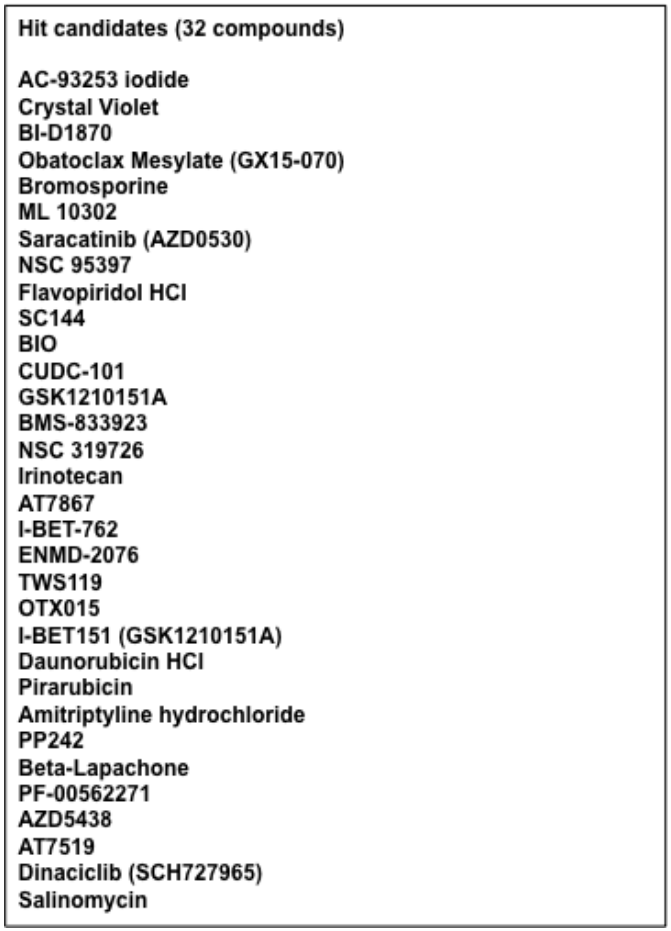

List of 32 candidate drugs from preliminary screening done in OVCAR3 *miR-181a* sensor sorted cells, which were further evaluated in secondary validation assays

Figure S6 *miR-181a* promoter acetylation

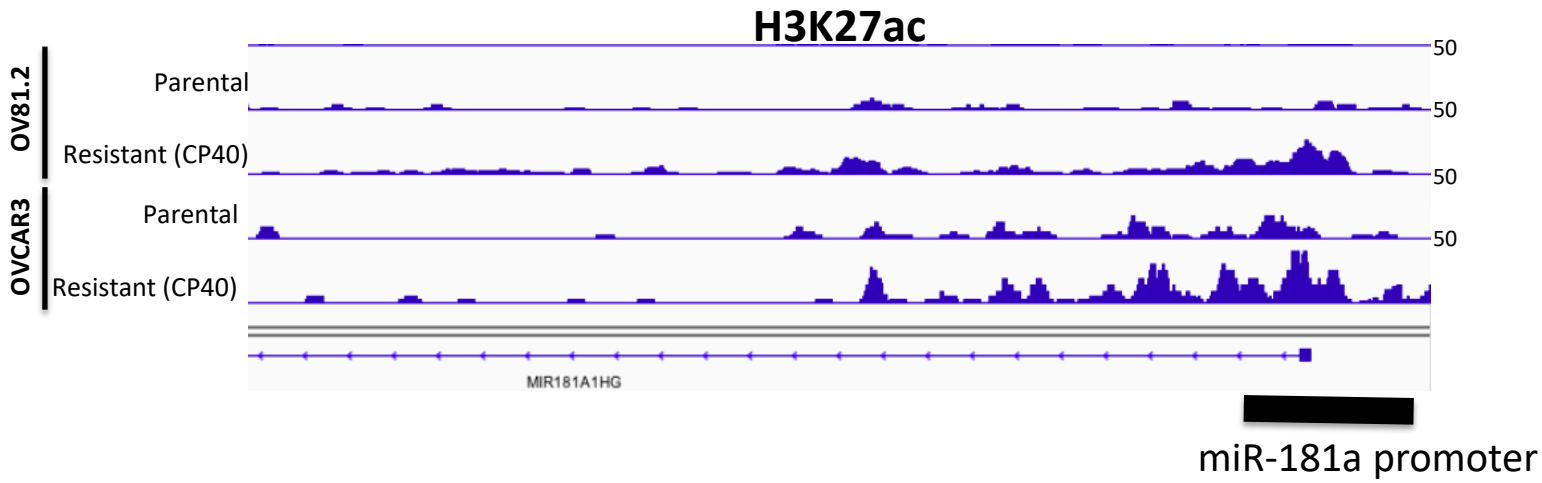

H3K27ac ChIP with rabbit anti-H3K27ac (Abcam no. 4729) was performed using 10 million cross-linked cells and sequencing libraries were prepared as previously described (Schmidt et al, Methods, 2009). ChIP–seq libraries were sequenced on a HiSeq 2500 platform at the Case Western Reserve University Genomics Core Facility. Data analysis was performed as previously described (Morrow et al, Nature Medicine 2018).

Supplementary Table 1 Identification of *miR-181a* predicted targets in top 100 downregulated genes in miR-181a ^{high} HGSOC cells : *miR-181a* predicted target list was downloaded the miRWalk database. Common genes between this list and the top 100 downregulated genes in *miR-181a* ^{high} HGSOC cells were analyzed to identify 27 potential miR-181a targets to be downregulated in miR-181a ^{high} HGSOC cells

Supplementary Table 2 *miR-181a* miRNA sensor-based high-throughput screen and validation of active hit candidates identified in *miR-181a* miRNA sensor-based high-throughput therapeutic screen : A total of 3114 mechanistically annotated partially redundant compounds were used for screening. Relative viability and mCherry FI were calculated for each well on per-plate basis. Top 32 compounds (approximately 1% of the library) were identified as potential hits using relative mCherry FI parameter. Upon hit identification, all compounds were validated as a stock solutions purchased from original vendor. Compound titration experiments demonstrated that eight compounds induce *miR-181a* miRNA sensor-driven mCherry FI in a specific and concentration-dependent manner.